AGU PUBLICATIONS

JGR

Journal of Geophysical Research: Solid Earth

RESEARCH ARTICLE
10.1002/2017JB013970

Key Points:
- We model friction evolution by keeping track of the heterogeneous strength of individual asperity contacts with an assumed size distribution
- If the strength of an asperity segment depends logarithmically on the velocity at which it formed, state evolution can mimic the slip law
- Equating "state" with "contact age" gives rise to state evolution that differs from the current aging law

Correspondence to:
T. Li,
tianyil@princeton.edu

Citation:
Li, T., and A. M. Rubin (2017), A microscopic model of rate and state friction evolution, *J. Geophys. Res. Solid Earth*, *122*, doi:10.1002/2017JB013970.

Received 12 JAN 2017
Accepted 14 JUL 2017
Accepted article online 18 JUL 2017

A microscopic model of rate and state friction evolution

Tianyi Li[1] **and Allan M. Rubin**[1]

[1] Department of Geosciences, Princeton University, Princeton, New Jersey, USA

Abstract Whether rate- and state-dependent friction evolution is primarily slip dependent or time dependent is not well resolved. Although slide-hold-slide experiments are traditionally interpreted as supporting the aging law, implying time-dependent evolution, recent studies show that this evidence is equivocal. In contrast, the slip law yields extremely good fits to velocity step experiments, although a clear physical picture for slip-dependent friction evolution is lacking. We propose a new microscopic model for rate and state friction evolution in which each asperity has a heterogeneous strength, with individual portions recording the velocity at which they became part of the contact. Assuming an exponential distribution of asperity sizes on the surface, the model produces results essentially similar to the slip law, yielding very good fits to velocity step experiments but not improving much the fits to slide-hold-slide experiments. A numerical kernel for the model is developed, and an analytical expression is obtained for perfect velocity steps, which differs from the slip law expression by a slow-decaying factor. By changing the quantity that determines the intrinsic strength, we use the same model structure to investigate aging-law-like time-dependent evolution. Assuming strength to increase logarithmically with contact age, for two different definitions of age we obtain results for velocity step increases significantly different from the aging law. Interestingly, a solution very close to the aging law is obtained if we apply a third definition of age that we consider to be nonphysical. This suggests that under the current aging law, the state variable is not synonymous with contact age.

1. Introduction

Decades of laboratory experiments have shown that friction in rock depends upon (1) the current sliding velocity and (2) the conditions on the sliding surface, which depend in part on the prior sliding history. This history dependence comprises the "state" part of "rate- and state-dependent friction" and is presumed to encompass properties such as contact area and contact quality [*Dieterich and Kilgore*, 1994; *Li et al.*, 2011]. A proper constitutive description of friction requires an equation for the evolution of this state. In the absence of a first-principles understanding, proposed laws have been based primarily on empirical fits to laboratory experiments, although recent attempts have been made to give such laws an underlying physical basis [*Sleep*, 2005; *Hatano*, 2015; *Perfettini and Molinari*, 2017].

Currently, the two most commonly used empirical descriptions of state evolution are termed the slip (Ruina) law and the aging (Dieterich) law [*Ruina*, 1983; *Marone*, 1998]. Both share the property that state does not evolve after the surface has slid long distances at constant velocity, where "long" is in comparison to some intrinsic length scale typically measured in microns. For small perturbations to steady sliding the two laws are asymptotically identical. Far from steady state significant differences arise. In particular, far "below" steady state, where state (and hence the "intrinsic strength") increases, the slip law implies that state increases only with slip, whereas the aging law implies that state increases with time even at zero slip speed. Following *Nakatani* [2001], by intrinsic strength we mean the strength of the surface at a reference slip speed, with units of stress ([shear force/area]).

Two categories of experiments have commonly been carried out to test these candidate laws: velocity step experiments and slide-hold-slide (SHS) experiments. It has long been known that velocity step data are fit very well by the slip law but very poorly by the aging law. The reason is that following the step, friction in these experiments can be characterized as evolving exponentially to its new steady state value over a characteristic slip distance that is independent of the size or sign of the step [e.g., *Bhattacharya et al.*, 2015]. This is precisely the slip law prediction. It is also entirely inconsistent with the aging law, which predicts healing with time

(and therefore healing over very short slip distances) following large velocity step decreases and linear slip weakening following large velocity step increases [*Dieterich and Kilgore*, 1996].

On the other hand, SHS data have long been interpreted as indicating time-dependent evolution during the holds. Although both the aging and the slip law reproduce the experimental observation that the peak stress upon resliding increases quasi-linearly with the logarithm of the hold time, the interpretation of time-dependent rather than slip-dependent healing received apparently strong support from the experiments of *Beeler et al.* [1994]. They found that the rate at which this peak stress increased was independent of the testing machine stiffness and, therefore, independent of the amount of surface slip during the load point hold. In addition, the see-through experiments of *Dieterich and Kilgore* [1994] demonstrated that contact area increases roughly as the logarithm of hold time for stationary surfaces. Given that state is commonly associated with contact area, rather than contact quality, these experiments were also interpreted as indicative of time-dependent healing of the surface, even in the limit of zero slip speed.

However, neither of the two laws can fit both velocity step and SHS experiments well, and the proper description of state evolution remains unknown after decades of research [*Marone*, 1998; *Karner and Marone*, 2001]. This uncertainty has implications for numerical models of earthquake nucleation, since the two laws can lead to very different nucleation styles [*Ampuero and Rubin*, 2008]. This dichotomy has also inspired modified versions of state evolution that encompass attributes of both the aging and slip laws [e.g., *Kato and Tullis*, 2001; *Nagata et al.*, 2012].

It is important to emphasize that the conclusion that healing in rock is time dependent is incompatible with the results of velocity step experiments, which show that healing following large velocity step decreases evolves with slip and not time [*Bhattacharya et al.*, 2015, 2016]. In addition, the conclusion that the data of *Beeler et al.* [1994] support time-dependent healing has recently been questioned [*Bhattacharya et al.*, 2017]. Given the equivocal nature of the *Beeler et al.* [1994] data, and the apparently unequivocal nature of velocity step data, in this study we set out to develop a kinematic picture of friction that is consistent with slip-dependent state evolution. In particular, we use as motivation the observation that following large velocity step decreases, healing does not proceed with time, as one would expect if state were contact area and individual contacts grew with time as seen by *Dieterich and Kilgore* [1994]. Instead, reaching a new steady state requires sliding a characteristic slip distance, as if this process requires swapping out all the old contacts in exchange for new ones, no matter how long this process takes [*Yoshioka and Iwasa*, 1996].

Here we explore a microscopic model of state in which each asperity has a heterogeneous intrinsic strength (state), with individual portions of contacts "remembering" the velocity at which they came into existence. Such a scenario could arise via any process that is much more efficient at the margin of a contact than within the interior. For example, *He et al.* [1999] and *Müser et al.* [2001] argue that the friction coefficient between arbitrary crystallographic cuts of the same or different pure minerals is essentially 0, because statistically there are as many atoms descending into potential energy wells as there are climbing out of them. In their model, frictional resistance comes from adsorbed impurities along the contact interface. If surface diffusion operates efficiently at the margins of contacts but not within the confined spaces of the contact interior, then the local impurity concentration within a contact could be set primarily by the concentration established when that portion of the contact slid into existence. This concentration will be slip speed dependent, with lower velocities allowing more time for chemical diffusion.

Because steady state friction is known to depend logarithmically on slip speed, we make the ad hoc assumption that the local intrinsic strength of a portion of an asperity depends on the logarithm of the velocity at which that portion came into being. Given that at any time two opposing portions of an asperity might have joined the contact at different slip speeds, we simply average the intrinsic strength of the two sides (plausible if the intrinsic strength is set by impurity concentration, for example). In keeping with current views of the direct velocity effect of friction [e.g., *Baumberger and Caroli*, 2006], we also assume that for a given intrinsic strength the resistance to sliding depends logarithmically on slip speed.

We develop a numerical kernel for friction evolution given an arbitrary slip history and a specified distribution of asperity diameters. For velocity steps, and an exponential distribution of asperity sizes, this model has an analytical solution that is similar to the slip law, and numerical inversions show that it performs as well as the slip law when fitting velocity step data. In addition, for arbitrary slip histories this model is not identical to the slip law, which is potentially useful, but unfortunately we find that it does not improve the fit to SHS data much.

Table 1. List of Mathematical Symbols and Their Descriptions

Symbol	Description
μ	friction coefficient
a	direct effect parameter
b'/b	microscopic/macroscopic evolution effect parameter
V	sliding velocity
θ/Θ	state parameter (traditional/in this study)
δ	slip (sliding) distance
k	spring stiffness
V_{lp}	load point velocity
σ	normal stress
τ	shear stress
D_c	characteristic length of asperity size distribution
A_c/A	real contact area/apparent area of the surface
N	total number of asperities on the surface
s	side length of a specific asperity size class
n_t	total areal asperity density on the surface
n_s	areal asperity density of size class s
$D_{\max}/D_{\min}$	the largest/smallest asperity size of the distribution
$\Delta\delta$	grid spacing
Ω	number of grid spacings of a size s asperity
$\hat{\tau}$	intrinsic strength of a grid element (units of stress)
$\hat{f}$	intrinsic fortitude of a grid element (units of force)
$\gamma_{s,k}$	summed intrinsic fortitude of an asperity contact (units of force)
$\tilde{\Gamma}_s$	averaged intrinsic strength of a size s asperity class (units of stress)
$\tilde{\Theta}$	intrinsic strength of the macroscopic friction surface (units of stress)
$\hat{t}$	contact age of a grid element
$\hat{t}_{\mathrm{asp}}$	average contact age of an entire asperity
α, K	exponent and normalizing factor of power law distribution

Because of the lingering uncertainty regarding the proper constitutive law for state evolution, we also use our model to explore scenarios under which the intrinsic strength of asperities increases as the logarithm of contact age. This of course is the standard interpretation of the aging evolution law [*Dieterich*, 1979; *Ruina*, 1983; *Linker and Dieterich*, 1992], the expectation being that contact area increases as the logarithm of time. However, while state for the aging law is sensibly equated with asperity age for long holds and during steady state sliding, it is not obvious that this is the case for general slip histories. For two plausible definitions of contact age, we obtain results that for velocity step increases are significantly closer to the slip law than to the aging law. Interestingly, we also find an analytical solution for velocity steps that is very close to the aging law, if we choose a third definition of age that we consider to be nonphysical.

The paper is organized as follows: In section 2 we summarize the standard rate and state friction equations and point out how our model differs in using a numerical kernel for the state evolution law. In section 3 we introduce the slip law-like version of our model, where the microscopic state at each location within a contact depends logarithmically on the velocity at which that location became part of the contact, and discuss how we determine the macroscopic surface state parameter from the underlying microscopic distribution. Further details, including analytical results for a velocity step, are given in Appendix B. In section 4 we undertake parameter inversions to determine how well this model can fit both velocity step and slide-hold-slide experiments. To investigate aging-law-like state evolution, where strength depends logarithmically on contact age, in section 5 we modify the original model to track the heterogeneous distribution of contact age rather than intrinsic strength. Different stress histories result depending upon whether and how one averages the microscopic ages prior to taking the logarithm. Additional details, including analytical results for a velocity step using one of these averaging strategies, are given in Appendix C. In section 6 we briefly discuss a few further

extensions of the model, prior to concluding in section 7. The mathematical symbols used in this paper are summarized in Table 1.

2. Rate and State Friction Equations

The rate and state friction equation can be written thus:

$$\mu = \mu_* + a \ln \frac{V}{V_*} + b \ln \frac{\theta}{\theta_*}\,; \tag{1a}$$

$$\mu = \mu_* + a \ln \frac{V}{V_*} + (\Theta - \Theta_*)\,. \tag{1b}$$

The μ is the friction coefficient (shear stress normalized by normal stress). Equation (1a) is the more common form [*Marone*, 1998]; (1b) is similar to that used by *Nakatani* [2001] and *Nakatani and Scholz* [2006]. In (1a), V is velocity, state θ has units of time (see below), and μ_* and θ_* are reference values of friction and state when sliding at steady state with an arbitrary reference velocity V_*. The parameters a and b are laboratory-derived parameters controlling the magnitude of the direct velocity effect and the state evolution effect, each of order 0.01, compared to a typical value of μ_* of 0.7. In (1b), state Θ is unitless, with steady state value Θ_* at the reference speed V_*.

In this study, we use (1b). The reason is that we prefer state to embody the change in intrinsic strength with changing contact history, as opposed to calling state "age" and assuming that we know how the intrinsic strength changes with contact age. The latter approach is the one typically taken when using (1a). Although in (1b) μ_* can be chosen to be identically Θ_* (eliminating both from the equation), we write μ_* to make the three components controlling the frictional strength (constant, direct effect, and state evolution effect) explicit. Taking the derivative of μ with respect to slip and multiplying by V, the differential form of (1b) is

$$V\frac{\mathrm{d}\mu}{\mathrm{d}\delta} = a\frac{\mathrm{d}V}{\mathrm{d}\delta} + V\frac{\mathrm{d}\Theta}{\mathrm{d}\delta}. \tag{2}$$

For a spring block slider being pulled with a load point velocity V_{lp}, the equation of elasticity for a spring with a finite stiffness k gives rise to (differentiating equation (25) of *Ruina* [1983], and normalizing k by the normal stress so that it has units of [length]$^{-1}$):

$$V\frac{\mathrm{d}\mu}{\mathrm{d}\delta} = k(V_{\mathrm{lp}} - V). \tag{3}$$

Given the history of V_{lp}, there are two unknowns (V, Θ), and a second equation that specifies the evolution of the state variable is required to determine the solution. For the state evolution laws currently in use, the time derivative of the state parameter in (1a) is given as a function of the current state and slip speed, $\dot{\theta} = f(V, \theta)$. The two most common versions are referred to as the "aging" law (4a) and the "slip" law (4b):

$$\dot{\theta} = 1 - \frac{V\theta}{D_c} \tag{4a}$$

$$\dot{\theta} = -\frac{V\theta}{D_c} \ln \frac{V\theta}{D_c}. \tag{4b}$$

As pointed out by *Ruina* [1983], not all description of state evolution can be written in the form $\dot{\theta} = f(V, \theta)$, and this is the case with our proposed model. The reason is that the same macroscopic value of state can arise from different microscopic distributions of intrinsic strength on the sliding surface, and these surfaces will evolve differently even for identical future slip histories $V(t)$. Thus, in our model, the state parameter depends upon the current state and the velocity history rather than only on the current state and velocity (as with the slip or aging law). Because in our model the current state also depends upon the velocity history, we can write the history dependence as $\Theta = F(V(\delta))$. The function F embodies a numerical scheme for tracking and summing the evolution of the state of individual grid elements and cannot be written in an analytical form. Equating (2) and (3), the complete equation set is

$$a\frac{\mathrm{d}V}{\mathrm{d}\delta} + V\frac{\mathrm{d}\Theta}{\mathrm{d}\delta} = k(V_{\mathrm{lp}} - V) \tag{5a}$$

$$\Theta = F(V(\delta)). \tag{5b}$$

Derivation of the numerical kernel F is described in section 3 and Appendix B.

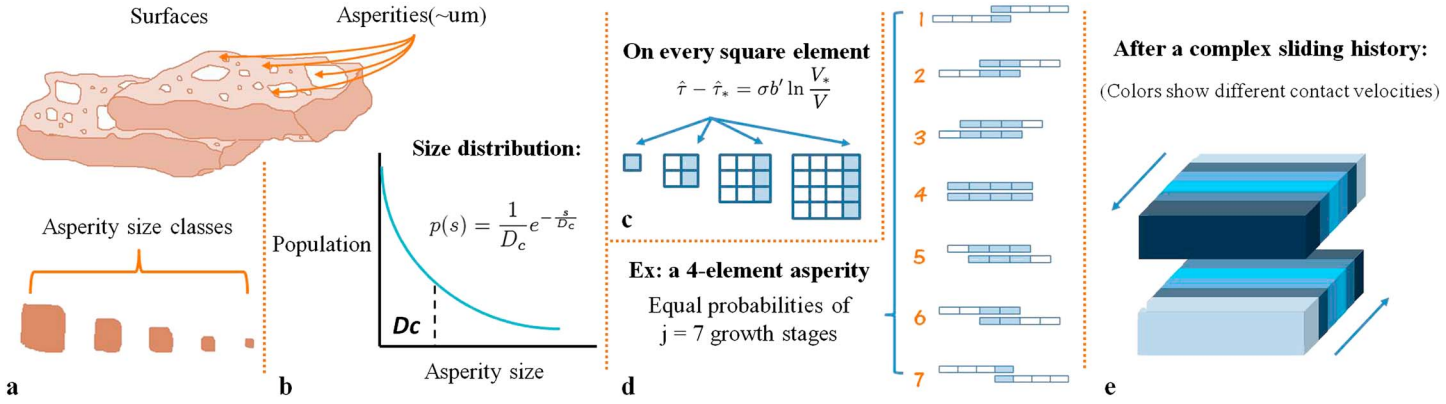

Figure 1. The microscopic picture and model assumptions for the implementation described in section 3.

3. Slip Law-Like Model

Deriving the numerical kernel F is a three-step procedure that consists of (1) adopting a particular set of rules that determine the intrinsic strength of an individual grid element, (2) tracking the intrinsic strength of each element from one slip step to the next as it enters, slides along, and eventually leaves a contact, and (3) summing the individual strengths of all grid elements within a representative sample of asperities on the sliding surface. The basic framework of our model allows us to vary the rules adopted in step (1) without changing much the structure of the underlying numerical code that tracks the evolution of individual elements and sums them over the sliding surface (steps 2 and 3). In this section we introduce the model using those rules that are designed to give it slip law-like behavior. In section 5 we modify these rules to generate aging-law-like behavior. Further variations of the model are also investigated and are presented in section 6.

3.1. Assumptions: The Microscopic Picture

Given a velocity step-down, slip-dependent healing implies that the approach to a new steady state requires that old contacts be destroyed and new ones formed, regardless of how slowly the surface is sliding. One scenario consistent with this requirement is to give individual portions of asperities an intrinsic strength that depends only upon the conditions at the time at which those portions came into being. We apply the following simplifying assumptions (Figure 1):

1. The velocity dependence of the intrinsic strength $\hat{\tau}$ of a single grid element is given by

$$\frac{\hat{\tau} - \hat{\tau_*}}{\sigma} = b' \ln \frac{V_*}{V_l}, \tag{6}$$

   where τ_* and V_* are arbitrary reference values (Figure 1c). We assume that the intrinsic strength depends logarithmically on the "initiation velocity" V_l because of the known velocity dependence of steady state friction. We further assume that individual grid elements will retain this initial strength during sliding and are not sensitive to subsequent velocity changes. This is the aspect of the model that gives rise to slip dependence. The coefficient b' is related to the macroscopic b in equation (1a) by

$$b = \frac{A_c}{A} b', \tag{7}$$

   where A_c and A are the real contact area and the apparent surface area, respectively (see Appendix B). Intuitively, the macroscopic b is a "diluted" value of the microscopic b' due to the fact that on the frictional surface only a small portion of the apparent area is in contact. We report our results in terms of b rather than b' in order to compare it with a and thus compare the direct and evolutionary effects.
2. The microscopic intrinsic strength at one location on the interface is the average of the two colocated elements of the two contacting asperities on opposite sides of the interface.
3. The probability of having an asperity with lateral length s on a macroscopic sliding surface is given by the exponential distribution (Figure 1b):

$$p(s) = \frac{1}{D_c} e^{-\frac{s}{D_c}}, \tag{8}$$

where D_c is the characteristic asperity length of the distribution. The exponential distribution is a reasonable distribution for natural materials, as is assumed in the Greenwood and Williamson picture of asperity heights between random surfaces [*Greenwood and Williamson*, 1966]. We consider power law distributions in section 6. In principle, the normalization of (8) extends to an infinite asperity size:

$$\int_0^\infty p(s)\mathrm{d}s = 1. \tag{9}$$

In practice, numerical considerations give rise to two additional parameters, the largest and smallest asperity sizes $D_{\max}$ and $D_{\min}$. $D_{\min}$ is set as one grid element spacing $\Delta\delta$. The above integral is discretized as

$$\sum_{D_{\min}/\Delta\delta=1}^{D_{\max}/\Delta\delta} p(\Omega) = 1, \tag{10}$$

where $\Omega = s/\Delta\delta$. We seek solutions in which (1) $\Delta\delta$ is small enough that further reductions do not affect the numerical results, and (2) $D_{\max}$ is large enough (far enough into the tail of the exponential distribution) that further increases also do not affect the numerical results (see section 4.1). In practice, $D_{\max}$ is several to a few tens of D_c.

4. Asperities are square, and the two contacting asperities are of equal size. Their edges in the slip-perpendicular direction are perfectly aligned (Figure 1e).
5. For each asperity size class, there is always a large number of asperities on a macroscopic surface, so that at one moment the probabilities of different stages of contact overlap between two asperities (illustrated in Figure 1d) are equal.

3.2. From an Asperity to the Surface

Relying on Assumption 1 (equation (6)), we define a microscopic intrinsic strength $\hat{\tau}(\Delta\delta)^2$, with units of force, of individual grid elements of side length $\Delta\delta$. To avoid ambiguity, in the following we use the designation "intrinsic fortitude" when the units are those of force, and intrinsic strength only when the units are those of stress. The macroscopic state Θ is then constructed from the summation of these intrinsic fortitudes. Consider a specific asperity size class with lateral length s, containing $\Omega = s/\Delta\delta$ grid spacings. Two asperities of this size class form a contact pair (Assumption 4, Figure 1e). The possible overlapping areas of the two asperities define $2\Omega - 1$ different stages of contact overlap in that size class (i.e., the overlapping length of asperities ranges from $\Delta\delta$ up to s and then back to $\Delta\delta$ again). At one instant, all of these stages are equally probable (Assumption 5, Figure 1d). The total intrinsic shear strength $\tilde{\Gamma}_s$ (units of stress) of this specific size class is defined as the summation of the intrinsic fortitude $\hat{\tau}(\Delta\delta)^2$ over the whole overlapped contact area, averaged over all the stages of overlap and multiplied by the number per area for that size class $n_s = n_t \cdot p(s)$, where n_t is the total asperity density of the surface (Appendix B):

$$\tilde{\Gamma}_s = n_s \frac{1}{2\Omega - 1} \sum_{\text{stages}} \sum_{\text{elements}} \hat{\tau} \cdot (\Delta\delta)^2. \tag{11}$$

The macroscopic shear strength $\tilde{\Theta}$ (units of stress) at the reference slip speed is computed over the whole spectrum of asperity sizes:

$$\tilde{\Theta} = \int_0^\infty \tilde{\Gamma}_s \mathrm{d}s. \tag{12}$$

The state parameter Θ is then constructed as $\Theta = \tilde{\Theta}/\sigma$. Under the definition of $\hat{\tau}$ (Assumption 1, Figure 1c), the steady state (subscript ss) sliding condition at constant V is satisfied ($\Theta_{ss}(V) - \Theta_{ss}(V_0) = b \ln V_0/V$), given the relation in (7) and the definition of the effective contact area A_c. Details of the summation process, the derivation of Θ during steady sliding, and $\mathrm{d}\Theta/\mathrm{d}\delta$ during velocity steps are given in Appendix B.

For a complicated sliding velocity history, there are a variety of values of $\hat{\tau}$ on different contacting elements due to their velocity history dependence. As a result, we are unable to find an analytical expression for the evolution of Θ as a function of slip for general sliding histories. Instead, a numerical kernel $F(V(\delta))$ is developed, using what we call an "evolution matrix" to track the evolution of state during sliding (Appendix B). Given an input of $V(\delta)$, $F(V(\delta))$ produces an output $\Theta(\delta)$ (equation (5b)).

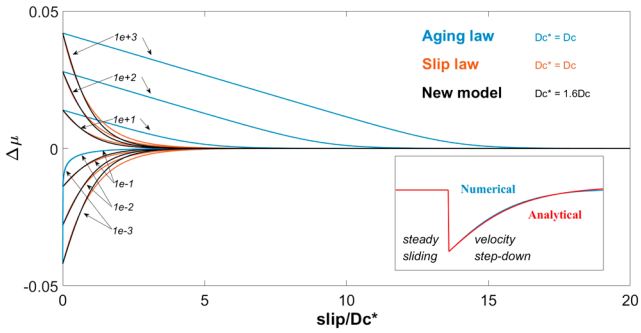

Figure 2. Comparison of friction evolution laws for velocity steps. Blue: aging law; red: slip law; black: slip law-like (new) model. Friction change $\Delta\mu$ is with respect to the future steady state value. Three step-ups ($1e+1/2/3$) and three step-downs ($1e-1/2/3$) are simulated. Inset: comparison of the analytical and numerical results for the new model (for the numerical results, $D_c^*/\Delta\delta = 30$ and $D_{max}/D_c^* = 7$).

3.3. Comparison With the Slip Law

Although we are unable to obtain an analytical expression for friction evolution for a completely general velocity history for the above model, there is an analytical expression for velocity steps on the surface. For a velocity step $V_0 \rightarrow V_1$, there is a resulting change in the elemental intrinsic strength $\hat{\tau}_0 \rightarrow \hat{\tau}_1$. Write $\Delta\hat{\tau} = \hat{\tau}_1 - \hat{\tau}_0$. Using the evolution matrix, the friction evolution with respect to slip δ after the velocity step can be tracked (Appendix B). Summing over all stages of overlap for a single asperity size class s, the strength $\tilde{\Gamma}_s$ decays linearly by $\Delta\hat{\tau}$ over a sliding distance s. Given an exponential distribution of asperity sizes, the strength of the surface $\tilde{\Theta}$ decays quasi-exponentially. In the limit of large $D_c/\Delta\delta$, an analytical result for the evolution of $\Theta = \tilde{\Theta}/\sigma$ is found to be

$$\frac{d\Theta}{d\delta} = \frac{b}{2D_c} \ln\frac{V_0}{V_1}\left(1+\frac{\delta}{D_c}\right)e^{-\frac{\delta}{D_c}}. \tag{13}$$

Integrating the above and putting the result into (1b), the friction evolution with respect to slip following the velocity step is given by

$$\mu = \mu_0 + \ln\frac{V_1}{V_0}\left\{a + b\left[\left(1+\frac{\delta}{2D_c}\right)e^{-\frac{\delta}{D_c}} - 1\right]\right\}. \tag{14}$$

For comparison, from (1a) and (4b) the equivalent result for the slip law is (Appendix B)

$$\mu = \mu_0 + \ln\frac{V_1}{V_0}\left\{a + b\left(e^{-\frac{\delta}{D_c}} - 1\right)\right\}. \tag{15}$$

Comparing (14) with (15), we see that for velocity steps, our model is essentially similar to the slip law except for the slip-dependent factor $(1+\delta/2D_c)$ modifying the exponential decay. We compare our new model with the slip law and the aging law for velocity steps in Figure 2. As with the slip law, and unlike the aging law, the new model is symmetric for velocity step-ups and step-downs and evolves over the same sliding distance for velocity steps of different magnitude. The response of the new model is basically similar to that of the slip law provided a scaling factor is applied to D_c (roughly, $D_c^{Slip} = 1.6D_c^{New}$). The inset shows the comparison between the analytical (equation (14)) and numerical results for the new model.

4. Inversion of Laboratory Friction Data

4.1. General Remarks

To test the model proposed in section 3, we use it to invert data from both large velocity step and SHS experiments. The velocity step data are from synthetic gouge from the Rock and Sediment Mechanics Lab, Penn State University [*Bhattacharya et al.*, 2015]; the SHS data are from initially bare granite from Brown University [*Beeler et al.*, 1994]. The main difference between our inversion and traditional inversions using the slip or aging law is that because of the underlying numerical grid, our numerical steps proceed in slip distance rather than time. For each computational step, the model slips by one grid element and the frictional quantities are then calculated for the new step. Therefore, we obtain a series of $V = V(\delta)$, $\Theta = \Theta(\delta)$, $\mu = \mu(\delta)$, and $t = t(\delta)$, where consecutive values of δ are separated by $\Delta\delta$, instead of $V = V(t)$, $\Theta = \Theta(t)$, $\mu = \mu(t)$, and $\delta = \delta(t)$. Inputs of $V_{lp}(\delta)$ are required to obtain $V(\delta)$. This is achieved by an interpolation process which transfers the data time series $V_{lp}(t)$ to the slip series $V_{lp}(n\Delta\delta)$ with the aid of $\delta = \delta(t)$. The sliding displacement $\delta(t)$ is calculated from the recorded load point displacement $\delta_{lp}(t)$ and friction $\mu(t)$ through the time-integrated form of equation (3): $\mu(t) = k(\delta_{lp}(t) - \delta(t))$, where k is the independently determined stiffness of the machine.

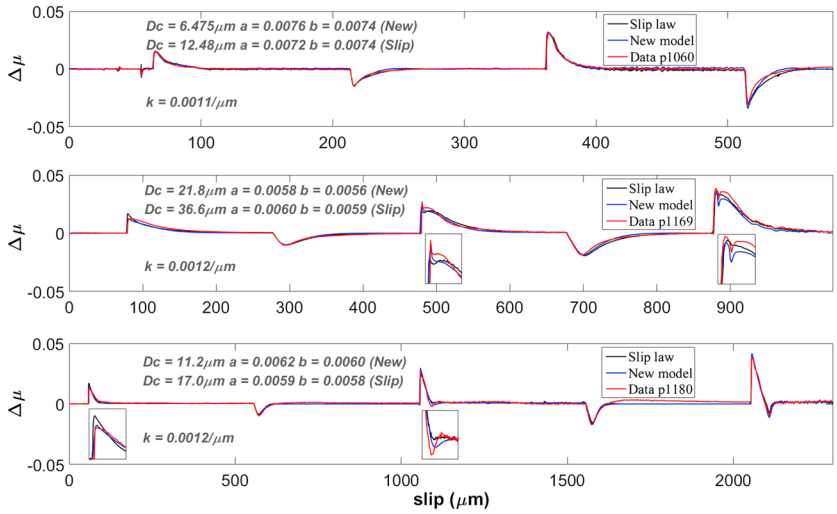

Figure 3. Inversion results for data p1060, p1169, and p1180, comparing the best fit of the slip law-like model with the best fit of the slip law (data from *Bhattacharya et al.* [2015]). The two best fit parameter sets are basically similar (with D_c scaled appropriately). The new model shows a slightly better performance for perturbations around some step-ups (insets). Numerical parameters: p1060: $D_{max}/D_c = 9.2$, $D_c/\Delta\delta = 25$; p1169: $D_{max}/D_c = 7.3$, $D_c/\Delta\delta = 44$; p1180: $D_{max}/D_c = 7.2$, $D_c/\Delta\delta = 28$. These ratios are large enough to not affect the numerical results.

Given the numerical requirements of $\Delta\delta \ll D_c$ and $D_{max} \gg D_c$, the number of asperity size classes $D_{max}/\Delta\delta$ is large. For velocity steps, we obtain convergence with $D_{max}/D_c \gtrsim 7$ and $D_c/\Delta\delta \gtrsim 25$; for SHS tests, a larger $D_c/\Delta\delta$ is required ($\gtrsim 40$), due to the fact that during the holds the sliding velocity is approaching 0 and a small slip distance embodies a large change in velocity (Figure A1). This large number of size classes prevents using time-consuming inversion methods such as Monte Carlo schemes. We use the downhill simplex method [*Press et al.*, 1986] to carry out the inversions in this study.

4.2. Velocity Step Experiments

Three experimental runs applying relatively large velocity steps of 1–3 orders of magnitude are considered (p1060, p1169, and p1180, from *Bhattacharya et al.* [2015, Figure 3]). Friction measurements were made on simulated granular quartz gouges at 25 MPa normal stress and room temperature and humidity. Relative sliding velocities ranged from 0.5 μm/s to 500 μm/s, and the sliding surface was close to velocity neutral ($a \sim b$). Previous results show that p1060 and p1180 are well fit by the slip law, while p1169 is fit slightly worse [*Bhattacharya et al.*, 2015]. Due to somewhat different experimental protocols, p1060 produced the most nearly "ideal" velocity steps on the sliding surface. One potential advantage of the new law is that because it is not identical to the slip law, it seems possible that it could fit the nonideal steps in p1169 better.

During the inversion, we fix the stiffness to the value derived from the earliest portion of the large velocity step increases [*Bhattacharya et al.*, 2015]. For each inversion, different starting parameters were applied for the downhill simplex method, and the same minimum misfit results were obtained (the starting parameters included those inferred by *Bhattacharya et al.* [2015] with D_c reduced by the expected factor of 1.6). Results show that for p1060, the new model fits the data well and is nearly identical to the best slip law fit; for p1169 and p1080, there is a suggestion that the new model performs slightly better for perturbations and overshoots near some steps, although it is generally similar to the slip law even for these nonideal velocity steps (Figure 3). Compared to the best fitting value of D_c for the slip law, D_c for the new model is larger by a factor of 1.68 for p1169 and 1.52 for p1180, close to the value of 1.6 anticipated for an ideal velocity step on the surface (Figure 2), but it is larger by a factor of 1.94 for p1060.

4.3. Slide-Hold-Slide Experiments

Because the new model can fit the velocity step data as well as the slip law, but is not identical to the slip law, we investigate whether it can fit the SHS data better than the slip law. We use the *Beeler et al.* [1994] data because the two different machine stiffnesses they used ($\sim$ 0.057/μm and 0.002/μm) are well suited to distinguish between slip-dependent and aging-law-like time-dependent healing. To invert the data, we fit only the stress minima at the end of each hold and the stress peaks after the reslide, rather than the whole

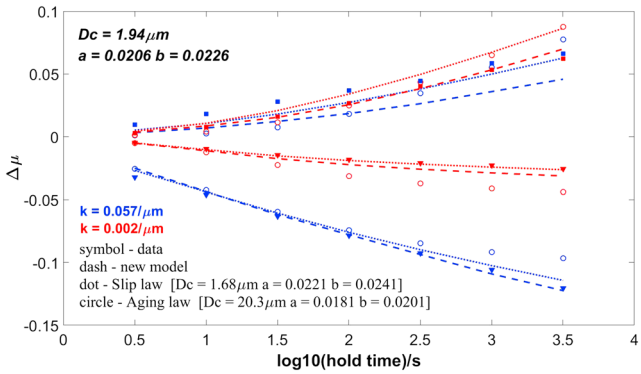

Figure 4. Inversion results for the SHS experiments of *Beeler et al.* [1994] (stress troughs and peaks), simultaneously inverting both high- and low-stiffness data. $a - b$ was fixed at −0.002 in the inversion based on velocity steps in the same experimental run. Symbols: data; dashed lines: best fit of the new model of section 3; dotted lines: best fit of the slip law; circles: best fit of the aging law. For the new model, $D_{max}/D_c = 7.3$, $D_c/\Delta\delta = 48$.

friction time series. We fit the high-stiffness and low-stiffness data using the same parameter values. In the experiments, the load point velocities are nominally set to 0 instantaneously at the start of the hold and instantaneously back to the steady sliding velocity V_0 at the end of the hold ($V_0 \sim 1$ μm/s for the lower stiffness and $V_0 \sim 0.3162$ μm/s for the higher stiffness apparatus). The inversion is carried out for such a perfect load point velocity input ($V_{lp} = 0$ or V_0). Tests show that the results are almost the same as inverting the real (nonperfect) load point velocity history. The motivation for using the idealized velocity history is that it lets us impose the start of the hold and the end of the hold when the block has slid integer multiples of the grid spacing $\Delta\delta$, whereas applying these velocity changes where they actually occurred in the experiments would introduce additional numerical error. A fixed $a - b = -0.002$ is also applied in the inversion, based on several velocity steps in the Beeler et al. data before the slide-hold-slide tests. Comparisons of the best fit of the new model with the best fits of the slip law and the aging law are shown in Figure 4. Data are shown by solid symbols (squares for stress peaks and triangles for the stress minima); the best fitting new model, slip law, and aging law are shown in colored dashed lines, colored dotted lines, and colored open circles, respectively. The new model shows a different best fit result from the slip law, and D_c is 1.15 times as large. When calculating a slip law series using the best fit parameters of the new model with the scaling factor 1.6 for D_c, the slip law results are also different from the new model (not shown). Both the best fit of the new model and the best fit of the slip law show a good fit to the stress minima while failing to match the stress peaks. The best fit of the aging law fails to match both the stress maxima and minima; it could do a better job of fitting the maxima at the expense of a much worse fit to the minima [*Bhattacharya et al.*, 2017]. We conclude that the new law does not significantly improve the fit to the SHS tests, relative to the slip law.

5. Is the Aging Law Really an "Aging Law"?

5.1. Idea of the Aging Law: Contact Age as State

Given that our slip-dependent evolution law does not fix the shortcomings of the slip law, we use our numerical procedure to investigate whether we can produce an aging law that more faithfully adheres to the underlying concept of "contact age." The traditional aging law combines equations (4a) and (1a). Integrating (4a) following an ideal velocity step increase on the sliding surface, state evolves exponentially with slip δ as $\theta = \theta_f + (\theta_i - \theta_f)e^{-\delta/D_c}$, where θ_i is the value of state prior to the step and θ_f is the steady state value of state long after the step. Because of the logarithm in (1a), for large velocity increases the stress decreases linearly out to slip distances much larger than D_c (Figure 2). This linear slip-weakening behavior is not observed in laboratory friction experiments [*Ruina*, 1983; *Nakatani*, 2001; *Bhattacharya et al.*, 2015] and is difficult to reconcile with the notion that friction evolves over a characteristic slip distance comparable to an asperity size [e.g., *Dieterich and Kilgore*, 1994, Figure 9].

Physical justifications of the aging law [e.g., *Brechet and Estrin*, 1994; *Baumberger and Caroli*, 2006] typically focus on the "1" on the right-hand side of (4a), which plausibly describes the logarithmic-with-time mushrooming of stationary contacts under high local normal stresses [*Dieterich and Kilgore*, 1994]. However, less theoretical attention has been paid to the $-V\theta/D_c$ term, which represents the destruction of state with slip and which is responsible for the long, linear decay of stress following large velocity increases when $V\theta/D_c \gg 1$. In fact, although the aging law sensibly describes contact age during long holds ($d\theta/dt \sim 1$, so $\theta \sim$ hold time) and at steady state ($d\theta/dt = 0 \rightarrow \theta = D_c/V$, where $D_c/V \sim$ contact lifetime), it is not at all clear that the

aging law describes contact age under more general slip histories. Our model is well suited to investigate this question, since it naturally can keep track of the local age of contacts as they are created and destroyed.

5.2. Different Definitions of Contact Age

In the standard interpretation of the aging law, state is identified as contact age, and strength depends logarithmically upon state. In terms of a physical picture, it is often pointed out that contact area grows logarithmically with time in indentation tests, consistent with the see-through experiments of *Dieterich and Kilgore* [1994] and with high-stress material flow laws [*Baumberger and Caroli*, 2006]. A self-consistent view is that small variations in the logarithm of contact age are proportional to small variations in true contact area and hence frictional strength. However, any process that allows the intrinsic strength of contacts to vary as log(time) would satisfy this picture, and increasing contact quality (e.g., via chemical diffusion) has also been cited as a possible mechanism of time-dependent frictional healing [*Li et al.*, 2011]. In our numerical scheme, the age $\hat{t}$ of a particular grid element at the end of a time step is given by

$$\hat{t} = \hat{t}_0 + \frac{\Delta\delta}{V}, \tag{16}$$

where $\hat{t}_0$ is the age at the start of the time step ($\hat{t}_0 = 0$ for the first grid elements of a particular asperity pair to overlap). We consider three strategies (one could devise more) for determining the intrinsic strength of the frictional interface, distinguished by whether and how these local ages are averaged prior to taking the logarithm:

Case A. The intrinsic strength (state) of each grid element is determined by the logarithm of the time since that element became part of the contact. In terms of a physical picture, one could imagine that when two square asperities of linear dimension s overlap by $\Delta\delta$, they acquire a nominal contact area of linear dimension $\Delta\delta$ in the slip direction and s in the slip-perpendicular direction, and that this area grows logarithmically with time in the slip-perpendicular direction. We consider the local age of the opposing surfaces forming the asperities separately and as before determine Θ by averaging the two sides. In the limit of arbitrarily small grid elements the element age becomes arbitrarily small, so one might anticipate the need to regularize the logarithm by using a cutoff time t_c [*Nakatani and Scholz*, 2006]. In this case the intrinsic strength of a grid element would be

$$\hat{\tau} = \hat{\tau}_0 + \sigma b' \ln\left(\frac{\hat{t}}{t_c} + 1\right). \tag{17}$$

In the limit of small ages, $\hat{t} \ll t_c$, this becomes $\hat{\tau} = \hat{\tau}_0$. For $\hat{t} \gg t_c$, $-b\ln(t_c)$ can be folded into the definition of $\hat{\tau}_0$, and (17) simplifies to

$$\hat{\tau} = \hat{\tau}_0 + \sigma b' \ln\left(\hat{t}\right). \tag{18}$$

For all elements with $\hat{t}_0 \gg t_c$ at the start of a time step, we can compute $\hat{\tau}$ at the end of the time step using (18). In addition, because $\int \log(t)\mathrm{d}t$ is well behaved even with a lower integration limit of $t = 0$, we can use (18) for all elements provided $\Delta\delta/V \gg t_c$, even when $\hat{t}_0 = 0$, and we enforce that criterion here. This intrinsic strength must then be weighted by element area and summed over all elements of all contact stages for each contact size class to determine Θ.

Case B. The intrinsic strength of each contact is determined by the logarithm of the average age of that contact:

$$\hat{\tau}_{\mathrm{asp}} = \hat{\tau}_0 + \sigma b' \ln\left(\hat{t}_{\mathrm{asp}}\right) \;;\; \hat{t}_{\mathrm{asp}} = \frac{1}{M}\sum_{i=1}^{M} \hat{t}_i\,, \tag{19}$$

where $\hat{t}_i$ is the age of each grid element within a contact consisting of M overlapping grid spacings in the slip direction. This intrinsic strength must then be weighted by contact area and summed over all contact stages and all contact size classes to determine Θ.

Case C. The intrinsic strength of the surface is determined by the logarithm of the average age of the surface, that is, the average of all the grid elements in all the contact stages of all the size classes. We view this definition of age as nonphysical, in that the intrinsic strength of a particular asperity depends upon the history of all the asperities on the surface, rather than its own history. Nonetheless, this case is interesting in that we are able to find an analytical solution for the stress evolution following a velocity step, unlike the more physical cases A and B, and for an exponential distribution of asperity sizes this solution is very similar to the traditional aging law. We have been unable to derive analytic solutions for velocity steps for cases A and B.

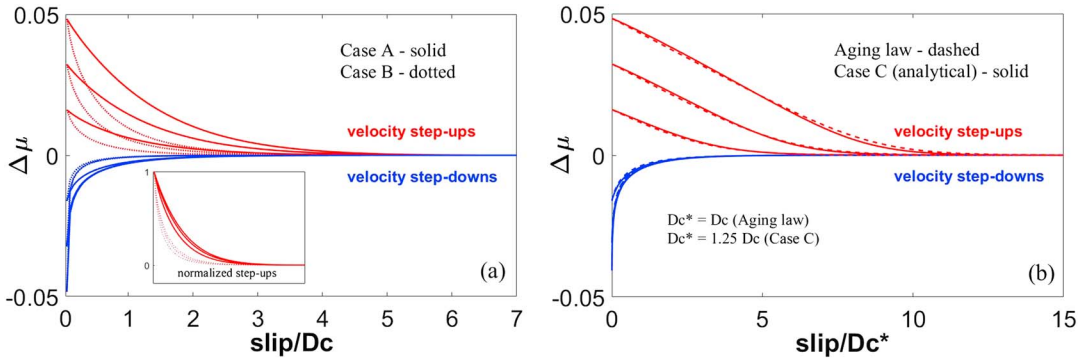

Figure 5. Three cases of the aging-like law of section 5. (a) Cases A and B (numerical, $D_c/\Delta\delta = 7$; $D_{max}/D_c = 25$); (b) case C (analytical) and the aging law. Note that in both cases A and B, the slope of the friction curve is not initially the same for velocity step-ups of different magnitudes. Inset: normalized step-ups for cases A and B. Larger velocity steps have slightly larger slip-weakening distances.

Numerical results for all three cases show, as expected, a large asymmetry between step velocity increases and decreases, with strengthening following large velocity decreases being primarily a function of time as existing asperities age, and weakening following large velocity increases being primarily a function of slip as existing asperities are destroyed and new ones formed (Figure 5). Following large velocity decreases, the numerical results appear qualitatively similar to the aging law. But following large velocity increases, the numerical results for cases A and B appear qualitatively more similar to the slip law, and to rock friction experiments, with stress decaying quasi-exponentially with slip rather than linearly. However, the slip scale for the stress decrease following velocity increases is not independent of the magnitude of the step, as it is for the slip law, but increases slightly as the step size increases (Figure 5a, inset). It is likely that existing experimental data are unable to distinguish such subtle differences.

For case C, we can obtain an analytical solution for a velocity step from V_0 to V_1 through a derivation similar to that for our slip-dependent law (Appendix C). Equations (13) and (14) now become

$$\frac{d\Theta}{d\delta} = \frac{1}{3D_c}\left(\frac{V_0}{V_1} - 1\right) h\left(\frac{\delta}{D_c}\right), \quad h(L) \equiv (L+2)e^{-L} \tag{20}$$

and

$$\mu = \mu_0 + a\ln\frac{V_1}{V_0} + b\ln\left[1 + \left(\frac{V_0}{V_1} - 1\right) H\left(\frac{\delta}{D_c}\right)\right], \quad H(L) \equiv 1 - \frac{L+3}{3}e^{-L}. \tag{21}$$

When $\delta \gg D_c$, $H(\delta/D_c) = 1$ and friction evolves to its steady state value, i.e., $\mu = \mu_0 + (a-b)\ln(V_1/V_0)$. The slope of the friction curve following a velocity step increase is

$$\frac{d\mu}{d\delta} = \frac{\frac{V_0}{V_1} - 1}{1 + \left(\frac{V_0}{V_1} - 1\right)\cdot H\left(\frac{\delta}{D_c}\right)} \frac{b}{D_c} \frac{\frac{\delta}{D_c} + 2}{3} e^{-\frac{\delta}{D_c}}. \tag{22}$$

At $\delta = 0$,

$$\frac{d\mu}{d\delta} = \frac{2b}{3D_c}\left(\frac{V_0}{V_1} - 1\right). \tag{23}$$

For large velocity increases ($V_0/V_1 \ll 1$), the initial slope of the friction curve is $-(2/3)b/D_c$, independent of the size of the step, compared to $-b/D_c$ for the aging law. Case C generates friction versus slip curves very similar to those for the aging law, using a value of D_c that is smaller than that of the aging law by a factor of 0.8. This is close to the value of 2/3 suggested by (23) but not identical because the slope $d\mu/d\delta$ evaluated at $\delta = 0$ does not extend unaltered to larger δ/D_c (Figure 5b).

6. Further Extensions of the Model

One benefit of the model is its versatility, which lets one explore hypotheses for state evolution with relative ease. Consider our slip law-like version: In the scheme we described in section 3, state on one side of the

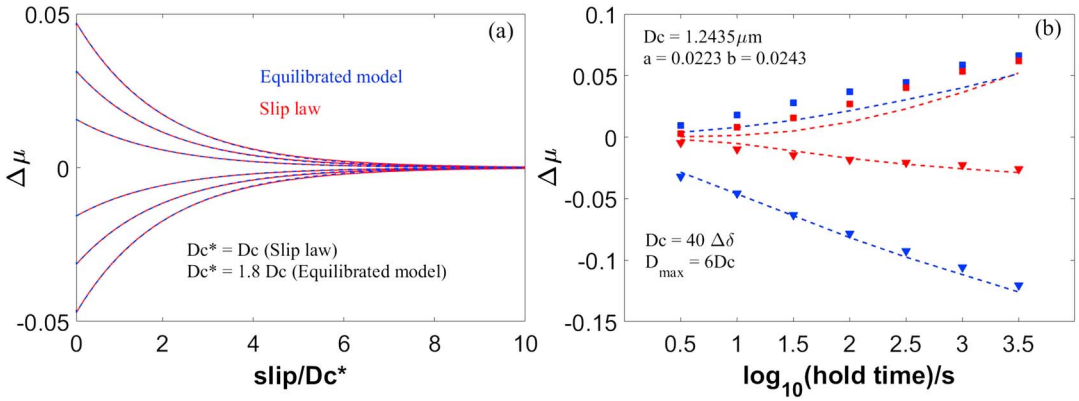

Figure 6. (a) Numerical results comparing the equilibrated model of section 6 and the slip law, with a scaling factor of 1.8 for D_c. For the equilibrated model, $D_c/\Delta\delta = 30$; $D_{max}/D_c = 7$. (b) Inversion results for the SHS data of *Beeler et al.* [1994] using the equilibrated model. Data of two stiffnesses are inverted simultaneously with $a - b = -0.002$ fixed.

contact is set by the velocity at which that grid element became part of the contact and is unchanged thereafter. But even if state is determined by diffusion of surface impurities, and this diffusion is easier at the margins of a contact than within the interior, one could still imagine that impurities easily hop from one side to another as the two surfaces slide past one another, allowing grid elements with different slip histories to equilibrate. For this reason we have explored a variant of this scheme where at each slip step we average the state of the juxtaposed elements on opposite sides of the interface. This does not change the macroscopic state of growing contacts, since it just redistributes state on a microscopic scale, but because of that redistribution it changes the macroscopic state evolution of shrinking contacts. Interestingly, we find numerically that for a velocity step this change makes the scheme ("equilibrated model") indistinguishable from the classical slip law, using a scaling factor of D_c(slip law) = 1.8D_c(equilibrated model) (Figure 6a). However, this equivalence does not extend to general slip histories, and we have been unable to obtain an analytical result for this variant. It is worth mentioning that this change yields a slightly better fit to the SHS data than the unequilibrated model (Figure 6b), in the sense that it is the only model to predict that the higher stiffness setup leads to higher peak stresses, as seen in the data (compare to Figure 4). Nonetheless, it seems premature to conclude that this is a good fit.

One can also maintain the same hypothesized microscopic mechanism of state evolution but vary the assumed asperity size distribution. For a power law, $p(s) \propto s^{-\alpha}$, we can again obtain analytical results for perfect velocity steps using the slip law-like model of section 3 (Appendix D):

$$\mu = \mu_0 + \ln\frac{V_1}{V_0}\left\{a - b\cdot\frac{3-\alpha}{2-\alpha}\cdot\frac{1}{D_{max}^{3-\alpha} - D_{min}^{3-\alpha}}\left[\frac{\alpha-2}{3-\alpha}D_{min}^{3-\alpha} + D_{max}^{2-\alpha}\delta - \frac{1}{3-\alpha}\delta^{3-\alpha}\right]\right\}, \quad (24)$$

where D_{min} and D_{max} are length scales specifying the limits of the power law distribution. For $D_{min} \ll D_{max}$, D_{min} becomes trivial when $\alpha < 3$, and D_{max} becomes trivial when $\alpha > 3$. In practice, for $\alpha < 3$, the behavior of the ensemble is dominated by the largest samples in the distribution, and D_{max} is roughly equal to the sliding distance over which the friction evolves. These solutions show that a power law asperity size distribution yields results similar but not identical to the exponential distribution, particularly for α in the vicinity of 2 (Figure 7). Note that "exponential" and "power law" distributions as applied here pertain to asperity size classes and not to the distribution of contact sizes at any one instant. For example, because each size class includes at least one scenario with a single overlapping grid element, the instantaneous distribution of contact sizes is skewed more heavily to small sizes than is the underlying asperity distribution. If desired, different underlying asperity size distributions could be devised so that the distribution of contacts is exponential, power law, etc.

As a final example of the model's versatility, we are currently exploring a scheme in which asperity contact area grows as log time, but where some slip is required for new contact area to reach full strength. One motivation is that contact area is known to increase even at zero slip speed [*Dieterich and Kilgore*, 1994]. In fact, this observation, together with the notion that variations in state reflect variations in true contact area, with a negligible role played by variations in contact quality, is one of the reasons that the aging law has become so popular in recent years. However, there is experimental support for the idea that quality matters [*Li et al.*, 2011], and, from

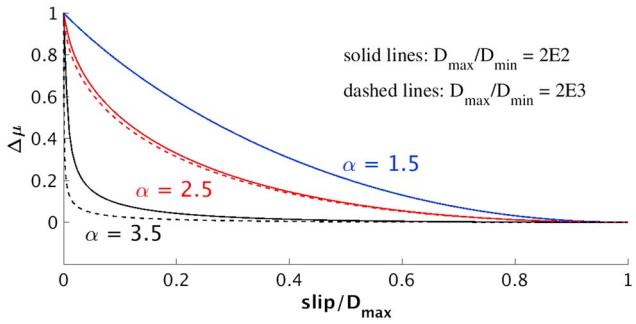

Figure 7. Analytical results for velocity steps (using the slip law-like model of section 3), assuming a power law distribution of asperity sizes for two D_{max}/D_{min} ratios (2E2 for solid lines; 2E3 for dashed lines) and three different values of α (1.5, 2.5, 3.5). Note that for $\alpha = 1.5$, the dashed and solid lines are indistinguishable.

normal stress step experiments, that new contact area is initially weak and requires slip or time to strengthen [*Linker and Dieterich*, 1992; *Hong and Marone*, 2005]. We find that incorporating both time-dependent and slip-dependent state evolution in this way provides a better fit to slide-hold-slide data than either the aging or slip laws, at the expense of fitting velocity step data worse than the slip law. It seems that the slip law matches velocity step data so well that it is difficult to make substantial changes to it without degrading that fit.

7. Discussion and Conclusions

The model described here establishes a clear two-scale physical picture for state evolution on a sliding interface. Starting from a hypothesized mechanism operating at the scale of the numerical grid, the model tracks the microscopic evolution of state between contacting asperities of equal size. The macroscopic state of the surface is then obtained by summing over all grid elements of all asperity size classes, weighted according to an assumed asperity size distribution. This approach has both advantages and disadvantages. One disadvantage is that the asperity size distribution on frictional interfaces is not well constrained, introducing (presumably within some bounds of reasonableness) an additional parameter. A second is that the assumptions that contacting asperities are of equal size and perfectly aligned in the slip-perpendicular direction are overly restrictive; future versions of the numerical method could relax this. A more difficult assumption to relax, from the standpoint of numerical discretization, is that circular or elliptical asperities seem more realistic than the square asperities we have assumed. Our hope, which seems reasonable, is that differences in asperity shape amount to only modest differences in model behavior relative to the gross features that we have focused on here.

An advantage of this approach is that the model allows one to investigate the macroscopic implications of a wide range of microscopic mechanisms for state evolution. Given that nearly all existing state evolution laws are entirely empirical, and that after decades of research no proposed state evolution law matches the full range of laboratory experiments, it seems worthwhile to explore evolution laws that cannot be written simply as functions of the current state and velocity [e.g., *Ruina*, 1983]. Moreover, because the model begins with a conception of what happens at the microscopic scale, any improvement in the fit to laboratory data carries with it the possibility that one has identified a mechanism (or at least the attributes of a mechanism) that contributes significantly to state.

Although slide-hold-slide data are equivocal [*Bhattacharya et al.*, 2017], and although zero stress holds show that some healing occurs at zero slip speed [*Nakatani and Mochizuki*, 1996], velocity step experiments clearly show that fault healing following large velocity decreases proceeds with slip and not time; that is, the same sliding distance is required to approach the new steady state, regardless of how long that takes [*Bhattacharya et al.*, 2015, 2016]. This sliding distance is plausibly a characteristic asperity dimension [*Dieterich and Kilgore*, 1994]. An interpretation consistent with these observations is that approaching a new steady state requires that old asperities be slid out of existence and new asperities created. But there is no well-established mechanism for generating such slip dependence. We examined the possibility that individual grid elements of asperities "remember" the velocity at which they entered the contact. Different physical or chemical processes could underly this behavior; diffusion of impurities that is easier at the margins than within the interiors of contacts is just one possibility. Assuming that the microscopic state varies inversely with the logarithm of the velocity at which that portion of the contact was created, and remains constant thereafter, and that the asperity size distribution is exponential, macroscopic behavior very similar to the classical slip law is produced. This realization of the model does as good a job as the slip law in fitting velocity step data but unfortunately is too similar to the slip law to improve the fit to slide-hold-slide data. For this realization we obtained analytical solutions for state and stress evolution following velocity steps but not for general slip histories.

The macroscopic implications of a given microscopic mechanism are not always obvious a priori. In the classical view of the friction equation (1a) and the aging evolution law (4a), state is equated with contact age [*Ruina*, 1983]. This view is consistent with the aging law far below steady state ($V\theta/D_c \ll 1 \Rightarrow \dot{\theta} \sim 1$) and at steady state ($V\theta/D_c = 1 \Rightarrow \theta = D_c/V$), but it is not at all obvious that this is the case above steady state ($V\theta/D_c > 1$). By modifying our scheme to equate state with contact age, and assuming frictional resistance to increase as the logarithm of state as in equation (1a), we can investigate this issue. Whether one takes the logarithm of the ages of all the grid elements and then sums them, or instead takes the logarithm of the average age of each asperity before summation, the resulting behavior is qualitatively similar to the classical aging law following large velocity decreases (fault healing is largely time dependent) but much more similar to the slip law following large velocity increases (fault weakening is largely slip dependent as old asperities are destroyed). Although we are not advocating for this state evolution law, as it does a much poorer job fitting velocity step data than the slip law, the results show that (1) state as embodied by the classical aging law does not represent contact age when the surface is well above steady state and the fault is weakening, and (2) this more faithful representation of contact age removes one glaring deficiency of the classical aging law, that being its linear slip-weakening behavior at constant slip speed well above steady state [*Bhattacharya et al.*, 2015].

Appendix A: Numerical Considerations and Stability Analysis

The two equations governing the evolution of friction are

$$a\frac{\mathrm{d}V}{\mathrm{d}\delta} + V\frac{\mathrm{d}\Theta}{\mathrm{d}\delta} = k(V_{\mathrm{lp}} - V) \tag{A1a}$$

and

$$\Theta = F(V(\delta)) \tag{A1b}$$

with unknowns V and Θ. We apply a semi-implicit scheme whose numerical form is

$$a\frac{V_i - V_{i-1}}{\Delta\delta} + V_i\frac{\Theta_i - \Theta_{i-1}}{\Delta\delta} = k\left(V_{\mathrm{lp},i} - \frac{V_{i-1} + V_i}{2}\right) \tag{A2a}$$

$$\Theta_i = F\left(\frac{V_{i-1} + V_i}{2}, V_{\mathrm{past}}\right). \tag{A2b}$$

In the above scheme, we applied an iterative procedure to enhance accuracy. For the first loop, the input of F in (A2b) is V_{i-1} instead of $(V_{i-1} + V_i)/2$. After Θ_i is calculated, V_i is obtained from (A2a) and is then put back into (A2b) to renew Θ_i. Only about four loops are required for convergence.

Rearranging (A2a),

$$V_i = \frac{\left(\frac{a}{\Delta\delta} - \frac{k}{2}\right)V_{i-1} + kV_{\mathrm{lp},i}}{\frac{a}{\Delta\delta} + \frac{k}{2} + \frac{\Theta_i - \Theta_{i-1}}{\Delta\delta}}. \tag{A3}$$

If $V < 0$, the numerical integration stops since the sliding velocity should be positive. Tests show that for the experiments we model and typical values of $\Delta\delta$, $(\frac{a}{\Delta\delta} + \frac{k}{2})$ is 1 order of magnitude larger than $|\frac{\Theta_i - \Theta_{i-1}}{\Delta\delta}|$, so the denominator of (A3) is always positive. Therefore, $V > 0$ requires

$$\begin{aligned} V_i > 0 &\Longrightarrow \left(\frac{a}{\Delta\delta} - \frac{k}{2}\right)V_{i-1} + kV_{\mathrm{lp},i} > 0 \\ &\Longrightarrow \frac{a}{k\Delta\delta} - \frac{1}{2} > -\frac{V_{\mathrm{lp},i}}{V_{i-1}}. \end{aligned} \tag{A4}$$

Using p1060 (Figure 3) as an example, for $a = 0.007$ and $k = 0.0011/\mu\mathrm{m}$, if $\Delta\delta = 0.3\,\mu\mathrm{m}$, the left-hand side of (A4) is ~ 20, which means that the numerical scheme will become unstable when $V_{\mathrm{lp},i}$ takes a very large negative value ($V_{\mathrm{lp},i}/V_{i-1} \lesssim -20$). Large negative values of V_{lp} occasionally arise in the data due to the imperfect nature of the servo control system. In our inversion, we ensure that $\Delta\delta$ is chosen to be small enough that $V_i > 0$.

Figure A1 shows how our numerical scheme converges, with increasing values of the maximum asperity size normalized by the grid spacing, for a representative slide-hold sequence.

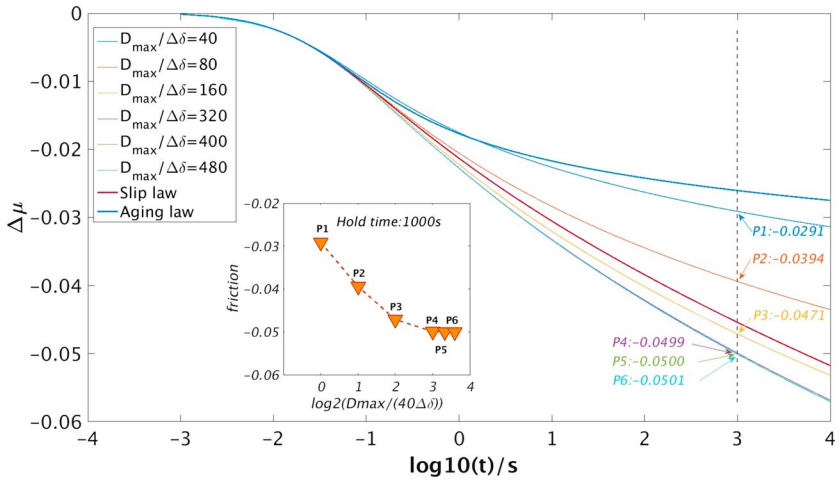

Figure A1. Convergence of simulation results for a hypothetical slide-hold sequence. For $D_{max}/\Delta\delta \gtrsim 300$ SHS friction curves converge, as a product of $D_{max}/D_c \simeq 7$ and $D_c/\Delta\delta \simeq 40$. For velocity steps, the constraint is slightly looser ($D_{max}/\Delta\delta \gtrsim 200$).

Appendix B: Constructing the Macroscopic State Parameter

Suppose the asperities are square, and that contacting asperities are of the same size and are perfectly aligned in the slip-perpendicular direction (Assumption 4). Consider a specific asperity size class with side length s. In the numerical scheme, we define a grid spacing $\Delta\delta$ on an asperity contact, also equivalent to the slip distance during one numerical step. An asperity of length s contains $\Omega = s/\Delta\delta$ grid spacings, which means that a fresh asperity of size s requires Ω slip increments to fully come into contact and other Ω slip increments to cease to exist.

If the total number of asperities is N over area A, the total areal density of asperities and the density of size class s are, respectively,

$$n_t = \frac{N}{A}; \quad n_s = n_t \cdot p(s). \tag{B1}$$

For any Ω, if the two contacting asperities always have the same side length s (Assumption 4), there are $k = 2\Omega - 1$ different contact stages (representing growing and shrinking contacts with different extents of overlap). The contact area grows for the first Ω stages ($k = 1, 2, \ldots\Omega$) and shrinks for the remaining $\Omega - 1$ stages ($k = \Omega + 1, \ldots, 2\Omega - 1$). We assume that there are equal numbers of all stages (Assumption 5):

$$n_{s,k=1\ldots2\Omega-1} = \frac{1}{2\Omega - 1} n_s = \frac{1}{2\Omega - 1} \cdot \frac{N}{A} p(s). \tag{B2}$$

The parameter $\hat{\tau}$ is defined as the microscopic intrinsic strength, meaning the strength of a single square grid element at a reference sliding speed, with units of stress. We use this concept to define a second intrinsic strength, this one with units of force, of a single grid element given by $\hat{f} = \hat{\tau} \cdot (\Delta\delta)^2$. To avoid ambiguity, we refer to an intrinsic strength that possesses units of force using the rather cumbersome designation intrinsic fortitude.

For each stage k, the summed contact intrinsic fortitude $\gamma_{s,k,\pm}$ is defined as the summation of $\hat{f}$ over all square grids on the overlapped contact area. The summation is carried out on both (+ and −) surfaces of the asperity contact.

$$\gamma_{s,k,\pm} = \sum_{\text{elements } \pm} \hat{f} = \sum_{\text{elements } \pm} \hat{\tau}(\Delta\delta)^2. \tag{B3}$$

The intrisic fortitude (for the kth stage) is averaged over the two surfaces:

$$\gamma_{s,k} = \frac{1}{2}(\gamma_{s,k,+} + \gamma_{s,k,-}). \tag{B4}$$

For simplicity, we drop the $\pm$ signs in the main text.

The intrinsic strength $\tilde{\Gamma}_s$ (units of stress) of an asperity size class s is obtained by summing the intrinsic fortitude of all the contact stages and multiplying by their areal density n_s:

$$\tilde{\Gamma}_s = \sum_{k=1}^{2\Omega-1} n_{s,k}\gamma_{s,k} = n_{s,k}\sum_{k=1}^{2\Omega-1}\gamma_{s,k} = n_s \cdot \frac{1}{2\Omega-1}\sum_{k=1}^{2\Omega-1}\gamma_{s,k}\,. \tag{B5}$$

The intrinsic strength of the macroscopic surface is computed over the whole spectrum of asperity sizes as

$$\tilde{\Theta} = \int_0^\infty \tilde{\Gamma}_s \mathrm{d}s. \tag{B6}$$

For steady sliding at the reference speed, $\tau_* = \tilde{\Theta}_* = \sigma\mu_*$; for steady sliding at a different speed,

$$\tau = \sigma\mu = \sigma a \ln(V/V_*) + \tilde{\Theta} \;=\; \tilde{\Theta}_* + \sigma a \ln(V/V_*) + (\tilde{\Theta} - \tilde{\Theta}_*)\,. \tag{B7}$$

The state parameter is thus constructed as

$$\Theta = \tilde{\Theta}/\sigma\,. \tag{B8}$$

Therefore, (B7) is equivalent to (1b) with μ_* equated with Θ_*:

$$\frac{\tau}{\sigma} = \mu = \mu_* + a\ln\frac{V}{V_*} + (\Theta - \Theta_*). \tag{B9}$$

B1. Steady State sliding

If grid elements have an intrinsic strength that depends only upon the velocity at which they became part of the contact, then during steady state sliding (constant V_0), all grid elements have the same microscopic strength:

$$\hat{\tau} = \hat{\tau_0}. \tag{B10}$$

Therefore,

$$\gamma_{s,k,+} = \gamma_{s,k,-} = \begin{cases} k\Omega\hat{\tau}_0(\Delta\delta)^2, & 0 < k \le \Omega \\ (2\Omega - k)\Omega\hat{\tau}_0(\Delta\delta)^2, & \Omega < k \le 2\Omega - 1 \end{cases} \tag{B11}$$

where one factor of Ω comes from the asperity length in the slip-perpendicular direction.

Summing over all the contact stages,

$$\sum_{k=1}^{2\Omega-1}\gamma_{s,k} = \Omega^3\hat{\tau}_0(\Delta\delta)^2\,. \tag{B12}$$

Then, for $\Omega \gg 1$ ($s \gg \Delta\delta$),

$$\tilde{\Gamma}_{s,0} = n_s \cdot \frac{1}{2\Omega-1}\Omega^3\hat{\tau}_0(\Delta\delta)^2 = \frac{s^2}{2}\hat{\tau}_0 \cdot n_s\,. \tag{B13}$$

Summing over the whole spectrum of contact sizes s,

$$\tilde{\Theta}_0 = \int_0^\infty \tilde{\Gamma}_{s,0}\mathrm{d}s = \int_0^\infty \frac{s^2}{2}\hat{\tau}_0 \cdot n_t\frac{1}{D_c}e^{-\frac{s}{D_c}}\mathrm{d}s = n_t\frac{D_c^2}{2}\hat{\tau}_0\int_0^\infty\left(\frac{s}{D_c}\right)^2 e^{-\frac{s}{D_c}}\mathrm{d}\frac{s}{D_c} = n_t D_c^2\hat{\tau}_0\,. \tag{B14}$$

If the sliding speed is the reference speed ($V_0 = V_*$), then $\tilde{\Theta}_0 = \tilde{\Theta}_*$. Note that

$$n_t D_c^2 = \frac{N}{A}D_c^2 = \frac{A_c}{A}\,, \tag{B15}$$

where

$$A_c = N\int_0^\infty \frac{s^2}{2}p(s)\mathrm{d}s = ND_c^2 \tag{B16}$$

is the real contact area of the surface. An asperity with side length s has the area s^2; however, at any moment, averaging all contact stages, only half of the asperity area is in contact, which gives rise to the factor of 1/2 in (B16).

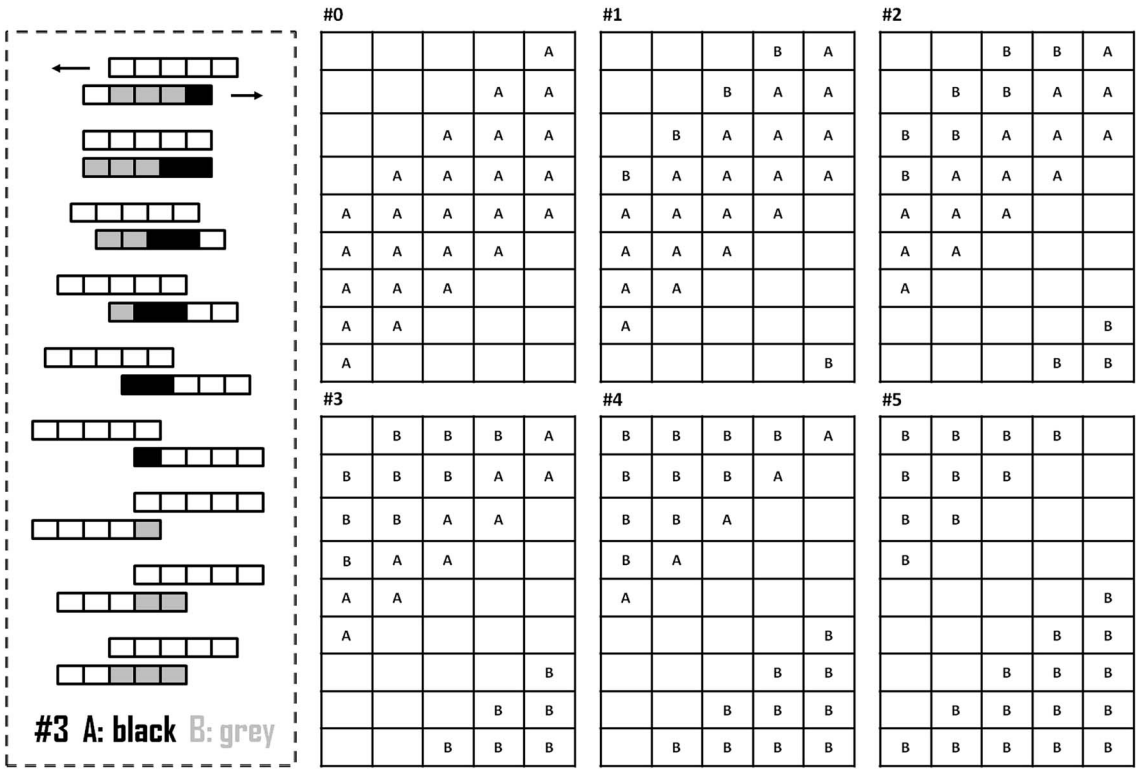

Figure B1. An example of the evolution of intrinsic strength for the slip law-like model (described in section 3 and Appendix B) after a velocity step, for an $\Omega = 5$ asperity. Each of the panels labeled #0–5 represents a snapshot in time of all the $2\Omega - 1 = 9$ contact stages (extent of asperity overlap at the time of the snapshot); each row of each panel represents one of these stages. Snapshot #0 is the steady state prior to the velocity step; #1 to #5 are the first Ω snapshots after the step $V_0 \rightarrow V_1$. For subsequent snapshots, there is no strength change. $A = \hat{\tau}_0$, $B = \hat{\tau}_1$. The graphic on the left shows diagrams of the two contacting asperities, for all nine stages corresponding to the nine rows in panel #3. The upper asperity moves to the left, the lower to the right. Black shading denotes A elements, gray shading B elements. Only the lower asperity of each contact is shaded to highlight the correspondence to the rows in panel #3.

Under two steady states sliding at different velocities V_1 and V_2, inserting into (B14) the equations (6) relating $\hat{\tau}$ to the microscopic b' and (7) relating the microscopic b' to the macroscopic b, we find

$$\Theta_2 - \Theta_1 = \frac{\tilde{\Theta}_2 - \tilde{\Theta}_1}{\sigma} = n_t D_c^2 (\hat{\tau}_2 - \hat{\tau}_1)/\sigma = \frac{A_c}{A} b' \ln \frac{V_1}{V_2} = b \ln \frac{V_1}{V_2}. \tag{B17}$$

Putting (B17) back in (1b), we see that the surface is steady state velocity neutral when $a = b$, as in standard rate and state friction.

B2. Velocity Steps

For a velocity step from $V_0 \rightarrow V_1$, there is a resulting change in $\hat{\tau}$, $\hat{\tau}_0 \rightarrow \hat{\tau}_1$. We write $\Delta\hat{\tau} = \hat{\tau}_1 - \hat{\tau}_0$. For each asperity size class s, this velocity change will be imposed on members currently at different stages of growth. Figure B1 shows how we track the slip-dependent evolution of contact strength for a representative sample of asperities of size class $\Omega = s/\Delta\delta = 5$. Each panel in this figure represents a different snapshot in time and each row in each panel a different contact stage (see figure caption for more details). Note that in this simplified model where the two contacting asperities have the same size, $\gamma_{s,k,+} = \gamma_{s,k,-} = \gamma_{s,k}$.

We need to record the evolution of $\gamma_{s,k}$. To achieve this, we formulate the matrix illustrated in Figure B2, which we term an evolution matrix, to track each growth stage that exists at the time of the velocity step through $2\Omega - 1$ slip steps. In this matrix, each row tracks the evolution with slip of one of $2\Omega - 1$ different contact stages present at the time of the velocity step; we refer to each of these $2\Omega - 1$ rows as following a different "scenario." Different columns in Figure B2 correspond to $2\Omega - 1$ consecutive snapshots, each taken at one time of all the scenarios. One column of Figure B2 corresponds to one full panel of Figure B1; each entry in that column corresponds to the sum of an entire row of the corresponding panel in Figure B1. Note that as illustrated in Figures B1 and B2, the snapshot of the final contact stage of a disappearing contact is always followed immediately by the snapshot of the first contact stage of a newly formed contact (in Figure B2 these

	1	2	3	...	Ω-1	Ω	Ω+1	...	2 Ω-3	2Ω-2	2 Ω-1
1	B	2B	3B		(Ω-1)B	ΩB	(Ω-1)B		3B	2B	B
2	B+A	2B+A	3B+A		(Ω-1)B+A	(Ω-1)B	(Ω-2)B		2B	B	B
3	B+2A	2B+2A	3B+2A		(Ω-2)B+A	(Ω-2)B	(Ω-3)B		B	B	2B
...											
Ω-1	B+(Ω-2)A	2B+(Ω-2)A	2B+(Ω-3)A		2B+A	2B	B		(Ω-4)B	(Ω-3)B	(Ω-2)B
Ω	B+(Ω-1)A	B+(Ω-2)A	B+(Ω-3)A		B+A	B	B		(Ω-3)B	(Ω-2)B	(Ω-1)B
Ω+1	(Ω-1)A	(Ω-2)A	(Ω-3)A		A	B	2B		(Ω-2)B	(Ω-1)B	ΩB
Ω+2	(Ω-2)A	(Ω-3)A	(Ω-4)A		B	2B	3B		(Ω-1)B	ΩB	(Ω-1)B
...											
2Ω-2	2A	A	B		(Ω-3)B	(Ω-2)B	(Ω-1)B		5B	4B	3B
2Ω-1	A	B	2B		(Ω-2)B	(Ω-1)B	ΩB		4B	3B	2B

Figure B2. The evolution matrix across a velocity step $V_0 \rightarrow V_1$, assuming a size Ω asperity pair having $2\Omega - 1$ contact scenarios (rows). The matrix keeps track of the evolution of intrinsic strength of asperity contacts over different contact scenarios (different rows) and time steps (different columns). One column of Figure B2 corresponds to one full panel of Figure B1; each entry in that column corresponds to the sum of an entire row of the corresponding panel in Figure B1. $A = \hat{\tau}_0$, $B = \hat{\tau}_1$. From one time step to the next (proceeding horizontally in the matrix), the asperity pair of a specific contact scenario (in a specific row) enters a new stage. Once the old contact pair (black) has slid out of existence, a new contact (red) is immediately formed to maintain constant contact area for that size class during sliding.

newly formed contacts are denoted by red text). This ensures that (1) the total contact area of a given asperity size class remains constant, and (2) at a given moment, all contact stages of a given size class are equally likely.

Using this matrix, we can calculate the summed strength over all contact scenarios (and hence all contact stages) for each snapshot. When inverting laboratory data, we do this for arbitrary slip histories, but here we continue to focus on velocity steps. In the following, numbers in brackets refer to scenarios (rows) and subscripts to snapshots (columns):

Snapshot 1 (Column 1)

$$\begin{aligned}\frac{\sum_{k=1}^{2\Omega-1}\gamma_{s,k}}{\Omega(\Delta\delta)^2} &= [1]_1 + [2]_1 + [3]_1 + \ldots + [2\Omega-2]_1 + [2\Omega-1]_1 \\ &= \Omega\hat{\tau}_1 + (\Omega^2-\Omega)\hat{\tau}_0 = \Omega^2\hat{\tau}_0 + \Omega(\hat{\tau}_1 - \hat{\tau}_0) = \Omega^2\hat{\tau}_0 + \Omega\Delta\hat{\tau}\end{aligned}$$

Snapshot 2 (Column 2)

$$\begin{aligned}\frac{\sum_{k=1}^{2\Omega-1}\gamma_{s,k}}{\Omega(\Delta\delta)^2} &= [1]_2 + [2]_2 + [3]_2 + \ldots + [2\Omega-2]_2 + [2\Omega-1]_2 \\ &= [1]_2 + [2]_2 + [3]_2 + \ldots + [2\Omega-2]_2 + [1]_1 \\ &= 2\Omega\hat{\tau}_1 + (\Omega^2-2\Omega)\hat{\tau}_0 = \Omega^2\hat{\tau}_0 + 2\Omega(\hat{\tau}_1 - \hat{\tau}_0) = \Omega^2\hat{\tau}_0 + 2\Omega\Delta\hat{\tau}\end{aligned}$$

Snapshot 3 (Column 3)

$$\begin{aligned}\frac{\sum_{k=1}^{2\Omega-1}\gamma_{s,k}}{\Omega(\Delta\delta)^2} &= [1]_3 + [2]_3 + [3]_3 + \ldots + [2\Omega-2]_3 + [2\Omega-1]_3 \\ &= [1]_3 + [2]_3 + [3]_3 + \ldots + [1]_1 + [1]_2 \\ &= 3\Omega\hat{\tau}_1 + (\Omega^2-3\Omega)\hat{\tau}_0 = \Omega^2\hat{\tau}_0 + 3\Omega(\hat{\tau}_1 - \hat{\tau}_0) = \Omega^2\hat{\tau}_0 + 3\Omega\Delta\hat{\tau}\end{aligned}$$

There are $2\Omega - 1$ snapshots in total. In the first Ω snapshots, the strength change summed over all the stages changes by $\Omega\Delta\hat{\tau} \cdot \Omega(\Delta\delta)^2 = s^2\Delta\hat{\tau}$ from each snapshot to the next:

$$\frac{\mathrm{d}\left(\sum_{k=1}^{2\Omega-1}\gamma_{s,k}\right)}{\mathrm{d}(\delta/\Delta\delta)} = s^2\Delta\hat{\tau}\,, \tag{B18}$$

which is linear with slip. During the next $\Omega - 1$ snapshots, the total strength for that size class remains unchanged.

For the first Ω snapshots,

$$\frac{\mathrm{d}\tilde{\Gamma}_s}{\mathrm{d}\delta} = n_s \cdot \frac{1}{2\Omega - 1} \frac{\mathrm{d}\left(\sum_{k=1}^{2\Omega-1} \gamma_{s,k}\right)}{\mathrm{d}\delta} = \frac{n_s}{2} \cdot s\Delta\hat{\tau}\,. \tag{B19}$$

Then we have

$$\frac{\mathrm{d}\tilde{\Gamma}_s}{\mathrm{d}\delta} = \begin{cases} \frac{n_s}{2} \cdot s\Delta\hat{\tau} & 0 < \delta \le s \\ 0 & s < \delta \end{cases}\,. \tag{B20}$$

Recalling (B6),

$$\frac{\mathrm{d}\tilde{\Theta}}{\mathrm{d}\delta} = \int_0^\infty \frac{\mathrm{d}\tilde{\Gamma}_s}{\mathrm{d}\delta}\mathrm{d}s = \int_\delta^\infty \frac{\mathrm{d}\tilde{\Gamma}_s}{\mathrm{d}\delta}\mathrm{d}s = \frac{n_t D_c^2 \Delta\hat{\tau}}{2D_c} e^{-\frac{\delta}{D_c}} \left(1 + \frac{\delta}{D_c}\right) = \frac{\tilde{\Theta}_1 - \tilde{\Theta}_0}{2D_c} e^{-\frac{\delta}{D_c}} \left(1 + \frac{\delta}{D_c}\right). \tag{B21}$$

Therefore,

$$\frac{\mathrm{d}\Theta}{\mathrm{d}\delta} = \frac{\mathrm{d}\tilde{\Theta}/\sigma}{\mathrm{d}\delta} = \frac{\Theta_1 - \Theta_0}{2D_c} e^{-\frac{\delta}{D_c}} \left(1 + \frac{\delta}{D_c}\right). \tag{B22}$$

Integrating the above equation,

$$\int_{\Theta_0}^{\Theta} \mathrm{d}\Theta = \frac{\Theta_1 - \Theta_0}{2} \int_0^\delta e^{-\frac{\delta}{D_c}} \left(1 + \frac{\delta}{D_c}\right) \mathrm{d}\left(\frac{\delta}{D_c}\right) \tag{B23}$$

$$\Longrightarrow \Theta - \Theta_0 = (\Theta_1 - \Theta_0)\left[1 - \left(1 + \frac{\delta}{2D_c}\right) e^{-\frac{\delta}{D_c}}\right]. \tag{B24}$$

Since $\Theta_1 - \Theta_0 = b\ln(V_0/V_1)$, plugging the above equation into (1b) and using V_0 as the reference speed, the evolution of friction following a velocity step is analytically

$$\begin{aligned} \mu &= \mu_0 + a\ln\frac{V_1}{V_0} + (\Theta_1 - \Theta_0)\left[1 - \left(1 + \frac{\delta}{2D_c}\right) e^{-\frac{\delta}{D_c}}\right] \\ &= \mu_0 + a\ln\frac{V_1}{V_0} + b\ln\frac{V_0}{V_1}\left[1 - \left(1 + \frac{\delta}{2D_c}\right) e^{-\frac{\delta}{D_c}}\right] \\ &= \mu_0 + \ln\frac{V_1}{V_0}\left\{a + b\left[\left(1 + \frac{\delta}{2D_c}\right) e^{-\frac{\delta}{D_c}} - 1\right]\right\}. \end{aligned} \tag{B25}$$

For a complicated velocity history, there are a variety of $\hat{\tau}$ on different grid elements, which denies an analytical expression for $\mathrm{d}\Theta/\mathrm{d}\delta$. However, the same form of the above matrix can be used to compute Θ by keeping track of the distribution of $\hat{\tau}$. Given an input series $V(\delta)$, an output series $\Theta(\delta)$ is produced; this is represented by the function F in equations (5b) and (A1b). Unfortunately, it should be noted here that by deriving a numerical kernel instead of a differential equation, we greatly complicate any numerical solution to the governing equations.

B3. Comparision With the Slip Law

The slip law is given by (4b) under the friction law (1a). Letting $\Theta = \ln\theta$, the slip law becomes (after a step to velocity V_1)

$$\frac{\mathrm{d}\Theta}{\mathrm{d}\delta} = -\frac{1}{D_c}(\Theta - \Theta_1)\,, \tag{B26}$$

where Θ_1 is the steady state Θ at the velocity V_1.

Integrating (B26),

$$\int_{\Theta_0}^{\Theta} \frac{\mathrm{d}\Theta}{\Theta - \Theta_1} = \int_0^\delta -\frac{\mathrm{d}\delta}{D_c} \tag{B27}$$

$$\begin{aligned} &\Longrightarrow \ln(\Theta - \Theta_1) - \ln(\Theta_0 - \Theta_1) = -\frac{\delta}{D_c} \\ &\Longrightarrow \Theta - \Theta_1 = e^{-\frac{\delta}{D_c}}(\Theta_0 - \Theta_1) \\ &\Longrightarrow \Theta - \Theta_0 = (e^{-\frac{\delta}{D_c}} - 1)(\Theta_0 - \Theta_1)\,. \end{aligned} \tag{B28}$$

Plugging into (1a), after a velocity step $V_0 \rightarrow V_1$

$$\begin{aligned}\mu &= \mu_0 + a\ln\frac{V_1}{V_0} + b(\Theta - \Theta_0)\\ &= \mu_0 + a\ln\frac{V_1}{V_0} + b(e^{-\delta/D_c} - 1)(\Theta_0 - \Theta_1)\\ &= \mu_0 + a\ln\frac{V_1}{V_0} + b\ln\frac{\theta_1}{\theta_0}(e^{-\delta/D_c} - 1)\\ &= \mu_0 + a\ln\frac{V_1}{V_0} + b\ln\frac{V_1}{V_0}(e^{-\delta/D_c} - 1)\\ &= \mu_0 + \ln\frac{V_1}{V_0}\left\{a + b\left(e^{-\delta/D_c} - 1\right)\right\}.\end{aligned} \tag{B29}$$

Appendix C: Aging-Law-Like Cases

C1. Velocity Neutrality Condition

We wish to compare steady state sliding at two velocities V_1 and V_2. For every grid element in the first case sliding at velocity V_1, and having a contact age $\hat{t}_1 = i\Delta\delta/V_1$, there is a corresponding grid element in the second case sliding at velocity V_2 with contact age $\hat{t}_1 = i\Delta\delta/V_2$, where i is some integer denoting the number of slip increments that grid element has undergone. Then the difference in intrinsic strength of the grid element at the two steady state sliding velocities is given by

$$\hat{\tau}_2 - \hat{\tau}_1 = \sigma b' \ln\frac{\hat{t}_2}{\hat{t}_1} = \sigma b' \ln\frac{i\Delta\delta/V_2}{i\Delta\delta/V_1} = \sigma b' \ln\frac{V_1}{V_2}. \tag{C1}$$

For case A, equation (C1) applies to every grid element on the surface and thus applies to their sum over the entire surface. As (C1) has the same form as equation (6) for the slip law-like model, equation (B17) in Appendix B applies as well and the velocity neutrality condition remains $a = b$. For case B, which averages the contact age of individual elements within each asperity before taking their logarithm, the $i\Delta\delta$ in (C1) becomes $(i\Delta\delta + j\Delta\delta + k\Delta\delta + \ldots)$ where $i, j, k\ldots$ are numbers of slip increments on different asperity portions, but the end result is the same and (B17) also holds true for case B. For case C we apply equation (1a) rather than (1b) and take the logarithm at the macroscopic scale to formulate the state variable Θ, in which case we have $\ln(\Theta_2/\Theta_1) = \ln(\sum\hat{t}_2/\sum\hat{t}_1) = \ln(V_2/V_1)$, and then $a = b$ naturally follows from the velocity neutral condition. Therefore, in our model, for all aging-law-like cases and the slip law-like case the surface is steady state velocity neutral when $a = b$.

C2. Response of Case C to a Velocity Step

Utilizing the evolution matrix and following the procedure discussed in Appendix B, corresponding analytical results for case C can be obtained. We continue to denote the state parameter as Θ, although physically it now corresponds to the θ in (1a). An example of the matrix evolution after a velocity step for an $\Omega = 5$ asperity is shown in Figure C1. Note that rather than tracking $\hat{\tau}$ we now track the grid element age $\hat{t}$. Carrying this forward, γ and Γ have units of [time·area], and $\tilde{\Theta}$ has units of [time]. At steady state (subfigure #0 in Figure C1), (B12)–(B14) become

$$\sum_{k=1}^{2\Omega-1}\gamma_{s,k} = \frac{1+\Omega}{2}\Omega^3\hat{t}_0(\Delta\delta)^2. \tag{C2}$$

For $\Omega \gg 1$ ($s \gg \Delta\delta$),

$$\tilde{\Gamma}_{s,0} = n_s \cdot \frac{1}{2\Omega - 1}\frac{1+\Omega}{2}\Omega^3\hat{t}_0(\Delta\delta)^2 = \frac{s^3}{4\Delta\delta}\hat{t}_0 \cdot n_s, \tag{C3}$$

and

$$\tilde{\Theta}_0 = \int_0^\infty \tilde{\Gamma}_{s,0}\mathrm{d}s = \frac{3}{2}n_t\frac{D_c^3}{\Delta\delta}\hat{t}_0 = \frac{3}{2}n_t\frac{D_c^3}{\Delta\delta}\cdot\frac{\Delta\delta}{V_0} = \frac{3}{2}n_tD_c^2\cdot\frac{D_c}{V_0}. \tag{C4}$$

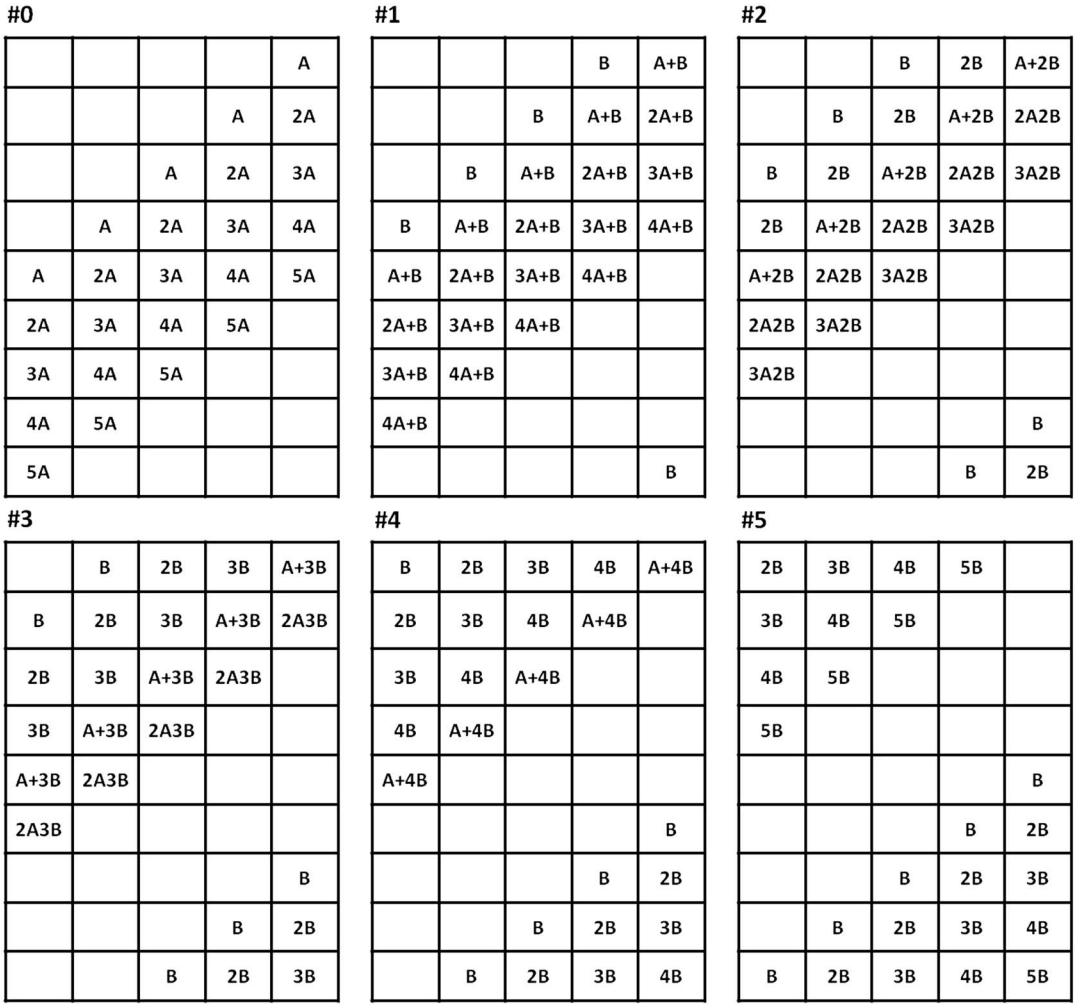

Figure C1. An example of the evolution of contact age distribution for the aging-like law after a velocity step, for an $\Omega = 5$ asperity (see Figure B1 for a fuller description). There are $2\Omega - 1 = 9$ stages. #0 is the prior steady state; #1 to #5 are the first Ω snapshots after the step $V_0 \to V_1$. $A = \hat{t}_0 = \Delta\delta/V_0$, $B = \hat{t}_1 = \Delta\delta/V_1$. In case A, we take the logarithm of each element as the local intrinsic strength; in case B, we take the logrithm of the average of each row (the average age of a single asperity); in case C, we take the logarithm on the macroscopic scale (the average contact age of all asperities on the surface).

For velocity steps, the state changes over the first Ω snapshots, and its change linearly decreases (#0–#5 in Figure C1). From the ith to the $(i+1)$th snapshot ($i = 0, 1, 2, \ldots, \Omega-1$), $\Omega(\Omega - i)$ old grid elements are replaced by new grid elements. (B20) and (B22) then become

$$\frac{\mathrm{d}\tilde{\Gamma}_s}{\mathrm{d}\delta} = \begin{cases} \frac{n_s}{2}\frac{s(s-\delta)}{\Delta\delta}\Delta\hat{t} = \frac{n_s}{2}\frac{s(s-\delta)}{\Delta\delta}\left(\frac{\Delta\delta}{V_0} - \frac{\Delta\delta}{V_1}\right) = \frac{n_s}{2}s(s-\delta)\frac{V_1 - V_0}{V_0 V_1} & 0 \le \delta \le s \\ 0 & s < \delta \end{cases} \tag{C5}$$

and

$$\frac{\mathrm{d}\Theta}{\mathrm{d}\delta} = \frac{1}{3D_c}\left(\frac{V_0}{V_1} - 1\right) \cdot h\left(\frac{\delta}{D_c}\right); \tag{C6}$$

$$h\left(\frac{\delta}{D_c}\right) = e^{-\frac{\delta}{D_c}}\left(\frac{\delta}{D_c} + 2\right), \tag{C7}$$

where $\Theta = \tilde{\Theta}/\tilde{\Theta}_0$. Integrating (C6),

$$\Theta - \Theta_0 = \left(\frac{V_0}{V_1} - 1\right) \cdot H\left(\frac{\delta}{D_c}\right); \tag{C8}$$

$$H\left(\frac{\delta}{D_c}\right) = 1 - \frac{\frac{\delta}{D_c} + 3}{3} e^{-\frac{\delta}{D_c}}. \tag{C9}$$

In this case, with contact age as the state parameter, we should take the logarithm of the state parameter and apply (1a) rather than (1b).

Setting $\Theta_0 = 1$ and plugging (C8) into (1a), now the evolution of friction following a velocity step becomes

$$\mu = \mu_0 + a \ln \frac{V_1}{V_0} + b \ln \left[1 + \left(\frac{V_0}{V_1} - 1 \right) \cdot H \left(\frac{\delta}{D_c} \right) \right] . \tag{C10}$$

When $\delta \gg D_c$, $H(\delta/D_c) \to 1$. Then the friction evolves to the steady state:

$$\mu = \mu_0 + a \ln \frac{V_1}{V_0} + b \ln \left[1 + \left(\frac{V_0}{V_1} - 1 \right) \right] = \mu_0 + (a-b) \ln \frac{V_1}{V_0} . \tag{C11}$$

The slope of the friction curve is

$$\frac{\mathrm{d}\mu}{\mathrm{d}\delta} = \frac{b}{\Theta} \frac{d\Theta}{d\delta} = \frac{\frac{V_0}{V_1} - 1}{1 + \left(\frac{V_0}{V_1} - 1 \right) \cdot H \left(\frac{\delta}{D_c} \right)} \frac{b}{D_c} \frac{\mathrm{d}H \left(\frac{\delta}{D_c} \right)}{\mathrm{d} \frac{\delta}{D_c}} = \frac{b}{\Theta} \frac{\frac{V_0}{V_1} - 1}{1 + \left(\frac{V_0}{V_1} - 1 \right) \cdot H \left(\frac{\delta}{D_c} \right)} \frac{b}{D_c} \frac{\frac{\delta}{D_c} + 2}{3} e^{-\frac{\delta}{D_c}} . \tag{C12}$$

At $\delta = 0$,

$$\frac{\mathrm{d}\mu}{\mathrm{d}\delta} = \frac{2b}{3D_c} \left(\frac{V_0}{V_1} - 1 \right) . \tag{C13}$$

For large velocity step-ups ($V_0/V_1 \ll 1$), the friction curves are near parallel, as for the aging law; for velocity step-ups and step-downs, the friction curves are asymmetric.

Appendix D: Power Law Asperity Size Distribution

Here we replace the assumption of an exponential distribution of asperity sizes with a power law distribution (with exponent α):

$$p(s) = K s^{-\alpha}, \; K = \frac{\alpha - 1}{D_{\min}^{1-\alpha} - D_{\max}^{1-\alpha}} , \tag{D1}$$

where K is the normalizing factor and $D_{\min}$ and $D_{\max}$ are parameters specifying the limits of the power law distribution.

For steady state sliding, (B14) becomes

$$\tilde{\Theta}_0 = n_t \frac{\hat{\tau}_0}{2} K \int_{D_{\min}}^{D_{\max}} s^{-\alpha+2} \mathrm{d}s = n_t \frac{\hat{\tau}_0}{2} K \frac{1}{3-\alpha} \left(D_{\min}^{3-\alpha} - D_{\max}^{3-\alpha} \right) . \tag{D2}$$

Following a velocity step, and assuming $D_{\min} < \delta$, (B22) becomes

$$\frac{\mathrm{d}\Theta}{\mathrm{d}\delta} = n_t \frac{\Delta\hat{\tau}}{2} K \int_{\delta}^{D_{\max}} s^{-\alpha+1} \mathrm{d}s = \frac{3-\alpha}{2-\alpha} \cdot \frac{\Theta_1 - \Theta_0}{D_{\max}^{3-\alpha} - D_{\min}^{3-\alpha}} \left(D_{\max}^{2-\alpha} - \delta^{2-\alpha} \right) . \tag{D3}$$

Integrating the above, (B24) and (B25) become

$$\Theta - \Theta_0 = \frac{3-\alpha}{2-\alpha} \cdot \frac{\Theta_1 - \Theta_0}{D_{\max}^{3-\alpha} - D_{\min}^{3-\alpha}} \left[\frac{\alpha - 2}{3-\alpha} D_{\min}^{3-\alpha} + D_{\max}^{2-\alpha} \delta - \frac{1}{3-\alpha} \delta^{3-\alpha} \right] \tag{D4}$$

and

$$\mu = \mu_0 + \ln \frac{V_1}{V_0} \left\{ a - b \cdot \frac{3-\alpha}{2-\alpha} \cdot \frac{1}{D_{\max}^{3-\alpha} - D_{\min}^{3-\alpha}} \left[\frac{\alpha - 2}{3-\alpha} D_{\min}^{3-\alpha} + D_{\max}^{2-\alpha} \delta - \frac{1}{3-\alpha} \delta^{3-\alpha} \right] \right\} \tag{D5}$$

for $D_{\min} \le \delta \le D_{\max}$.

Acknowledgments
Tianyi thanks Pathikrit Bhattacharya for his sincere instructions and valuable discussion on rate and state friction. We thank Masao Nakatani for his extremely valuable reviews and important suggestions, which went above and beyond the call of duty and substantially improved the paper, and one anonymous reviewer for comments that helped with organization and clarity. All data used in this study are available upon request from the authors. This research was funded by the National Science Foundation under award EAR-1547286, and by the U.S. Geological Survey (USGS), Department of the Interior, under USGS award G16AP00028. The views and conclusions contained in this document are those of the authors and should not be interpreted as necessarily representing the official policies, either expressed or implied, of the U.S. Government.

References

Ampuero, J.-P., and A. M. Rubin (2008), Earthquake nucleation on rate and state faults—Aging and slip laws, *J. Geophys. Res.*, *113*, B01302, doi:10.1029/2007JB005082.

Baumberger, T., and C. Caroli (2006), Solid friction from stick–slip down to pinning and aging, *Adv. Phys.*, *55*(3–4), 279–348.

Brechet, Y., and Y. Estrin (1994), The effect of strain rate sensitivity on dynamic friction of metals, *Scr. Metall. Mater.*, *30*(11), 1449–1454.

Beeler, N., T. Tullis, and J. Weeks (1994), The roles of time and displacement in the evolution effect in rock friction, *Geophys. Res. Lett.*, *21*(18), 1987–1990.

Bhattacharya, P., A. M. Rubin, E. Bayart, H. M. Savage, and C. Marone (2015), Critical evaluation of state evolution laws in rate and state friction: Fitting large velocity steps in simulated fault gouge with time-, slip-, and stress-dependent constitutive laws, *J. Geophys. Res. Solid Earth*, *120*, 6365–6385, doi:10.1002/2015JB012437.

Bhattacharya, P., A. M. Rubin, T. Tullis, K. Okazaki, and N. M. Beeler (2016), Where did the time go? Friction evolves with slip following large velocity steps, normal stress steps and during long holds, Abstract S14B-08 presented at 2016 Fall Meeting, Physics of Earthquake Rupture Propagation, AGU, San Francisco, Calif.

Bhattacharya, P., A. M. Rubin, and N. M. Beeler (2017), Does fault strengthening in laboratory rock friction experiments really depend primarily upon time and not slip?, *J. Geophys. Res. Solid Earth*, *122*, doi:10.1002/2017JB013936.

Dieterich, J. H. (1979), Modeling of rock friction: 1. Experimental results and constitutive equations, *J. Geophys. Res.*, *84*(B5), 2161–2168.

Dieterich, J. H., and B. Kilgore (1996), Implications of fault constitutive properties for earthquake prediction, *Proc. Natl. Acad. Sci.*, *93*(9), 3787–3794.

Dieterich, J. H., and B. D. Kilgore (1994), Direct observation of frictional contacts: New insights for state-dependent properties, *Pure Appl. Geophys.*, *143*(1–3), 283–302.

Greenwood, J., and J. Williamson (1966), Contact of nominally flat surfaces, *Proc. R. Soc. London, Ser. A*, *295*, 300–319.

Hatano, T. (2015), Friction laws from dimensional-analysis point of view, *Geophys. J. Int.*, *202*(3), 2159–2162.

He, G., M. H. Müser, and M. O. Robbins (1999), Adsorbed layers and the origin of static friction, *Science*, *284*(5420), 1650–1652.

Hong, T., and C. Marone (2005), Effects of normal stress perturbations on the frictional properties of simulated faults, *Geochem. Geophys. Geosyst.*, *6*(3), Q03012, doi:10.1029/2004GC000821.

Karner, S. L., and C. Marone (2001), Frictional restrengthening in simulated fault gouge: Effect of shear load perturbations, *J. Geophys. Res.*, *106*(B9), 19–319.

Kato, N., and T. E. Tullis (2001), A composite rate-and state-dependent law for rock friction, *Geophys. Res. Lett.*, *28*(6), 1103–1106.

Li, Q., Y. Dong, D. Perez, A. Martini, and R. W. Carpick (2011), Speed dependence of atomic stick-slip friction in optimally matched experiments and molecular dynamics simulations, *Phys. Rev. Lett.*, *106*(12), 126101.

Linker, M., and J. Dieterich (1992), Effects of variable normal stress on rock friction: Observations and constitutive equations, *J. Geophys. Res.*, *97*(B4), 4923–4940.

Marone, C. (1998), The effect of loading rate on static friction and the rate of fault healing during the earthquake cycle, *Nature*, *391*(6662), 69–72.

Müser, M. H., L. Wenning, and M. O. Robbins (2001), Simple microscopic theory of Amontons's laws for static friction, *Phys. Rev. Lett.*, *86*(7), 1295.

Nagata, K., M. Nakatani, and S. Yoshida (2012), A revised rate-and state-dependent friction law obtained by constraining constitutive and evolution laws separately with laboratory data, *J. Geophys. Res.*, *117*, B02314, doi:10.1029/2011JB008818.

Nakatani, M. (2001), Conceptual and physical clarification of rate and state friction: Frictional sliding as a thermally activated rheology, *J. Geophys. Res.*, *106*(B7), 13,347–13,380.

Nakatani, M., and H. Mochizuki (1996), Effects of shear stress applied to surfaces in stationary contact on rock friction, *Geophys. Res. Lett.*, *23*(8), 869–872.

Nakatani, M., and C. H. Scholz (2006), Intrinsic and apparent short-time limits for fault healing: Theory, observations, and implications for velocity-dependent friction, *J. Geophys. Res.*, *111*, B12208, doi:10.1029/2005JB004096.

Perfettini, H., and A. Molinari (2017), A micromechanical model of rate and state friction: 1. Static and dynamic sliding, *J. Geophys. Res. Solid Earth*, *122*, 2590–2637, doi:10.1002/2016JB013302.

Press, W. H., S. A. Teukolsky, W. T. Vetterling, and B. P. Flannery (1986), Downhill simplex method in multidimensions, in *Numerical Recipes: The Art of Scientific Computing*, 3rd, vol. 10, pp. 289–293, Cambridge Univ. Press, New York.

Ruina, A. (1983), Slip instability and state variable friction laws, *J. Geophys. Res.*, *88*(B12), 10,359–10,370.

Sleep, N. H. (2005), Physical basis of evolution laws for rate and state friction, *Geochem. Geophys. Geosyst.*, *6*, Q11008, doi:10.1029/2005GC000991.

Yoshioka, N., and K. Iwasa (1996), The characteristic displacement in rate and state-dependent friction from a micromechanical point of view, *Pure Appl. Geophys.*, *147*(3), 433–453.